NUMERICAL MODELING FOR CHARACTERIZATION OF PEBBLE BED REACTOR BYPASS FLOWS

A Thesis

by

NOLAN ERIC MACDONALD

Submitted to the Office of Graduate and Professional Studies of
Texas A&M University
in partial fulfillment of the requirements for the degree of

MASTER OF SCIENCE

Chair of Committee,	Mark L. Kimber
Committee Members,	Karen Vierow Kirkland
	Maria King
Head of Department,	Michael Nastasi

August 2021

Major Subject: Nuclear Engineering

ABSTRACT

High-Temperature Gas-Cooled Reactor (HTGR) concepts are Gen-IV reactor designs distinguished by a high level of technology readiness, walk-away safety, and high coolant outlet temperatures. All developed HTGR designs can be categorized into two concepts, the prismatic reactor and pebble bed reactor (PBR). The prismatic reactor core is comprised of hexagonal graphite blocks with cylindrical borings that contain cylindrical fuel compacts or coolant flow; alternatively, the pebble bed concept fuel is encapsulated by tennis-ball sized spherical graphite pebbles that move through the reactor bed under gravity. Encompassing both core designs are graphite reflector blocks that are distributed with small radial and axial gaps to mitigate any additional stresses from thermal expansion. These gaps form secondary coolant flow paths that may allow a significant amount of the coolant to bypass the core increasing the core peak fuel temperature. For this reason, a relevant full core analysis must take into account all the bypass flow, including secondary and leakage flow paths.

Higher order numerical analysis of flow patterns in HTGR concepts can be performed using Computational Fluid Dynamics (CFD), however, considering the complexity of the geometry and the duration of some safety related transients, CFD modeling would require a prohibitive amount of computational resources. A computationally efficient approach would be using a lower-fidelity thermal-hydraulics code such as Pronghorn. Pronghorn is a coarse-mesh, multi-dimensional, thermal-hydraulic (T/H) simulation tool developed by Idaho National Laboratory (INL) using the Multiphysics Object-Oriented Simulation Environment (MOOSE) framework. T/H codes such as Pronghorn can be an effective solution, however, they lack the ability to account for local phenomena and important characteristics of bypass flow. In order to establish these capabilities in Pronghorn, CFD steady state simulations can be utilized to create correlations for implementation in Pronghorn. This two-step approach uses higher-fidelity CFD methodology to inform Pronghorn, resulting in a computationally efficient simulation tool able to capture the relevant phenomena. Consequently, Pronghorn will be able to run safety related transients maintaining a

good level of accuracy but drastically reducing the computational time.

The proposed research aims to employ a two-step approach with CFD models of representative PBR geometries used to derive an ad-hoc approach for Pronghorn in order to correctly predict the mass redistribution within the reactor with a model capable of running on a workstation within minutes. The present investigation sets out to develop a representative two-dimensional PBR model based on the HTR-10, a 10 MWt prototype pebble bed reactor. The representative two-dimensional, axisymmetric model includes secondary flow paths and employs the commercial finite volume CFD software, STAR-CCM+, to form a training dataset for a Pronghorn model of the same geometry. Multiple gap sizes and flow conditions have been investigated to generalize the approach that will be utilized in Pronghorn to demonstrate feasibility of computing bypass flow. Ultimately, a PBR bypass flow investigation is conducted using Pronghorn to explore the effects of bypass flow on PBR phenomena. This research sets the groundwork for future studies aimed at high accuracy validation efforts, which will further enhance the utility of contributions made in the present study regarding PBR bypass flow phenomena.

ACKNOWLEDGMENTS

I would like to thank my committee chair and acadmic advisor, Dr. Mark Kimber, for the guidance and support not only throughout the entirety of this research process, but for a majority of my undergraduate and graduate academic career in the Texas A&M University Nuclear Engineering Department. Additionally, I would like to thank my committee members, Dr. Karen Vierow Kirkland and Dr. Maria King for their guidance and support while conducting my thesis research.

I would like to give a special thanks to Sebastian Schunert and Paolo Balestra at Idaho National Laboratory for giving me the opportunity to work and develop alongside their guidance, as well as continuously providing any feedback needed throughout my research. I also would like to especially thank my friends and colleagues at Texas A&M University, specifically, Dr. Corey E. Clifford, Dr. Austen D. Fradeneck, Dr. Adam M. Oler, Ramiro Freile, Andrew Hermosillo and Begoña Aranguren for their infinite amount of support, advice, and guidance to make all of this possible.

Lastly, the unwavering support and motivation provided by my family is appreciated more than words can express. To my father, thank you for serving as a foundation I could always lean on. To my grandmother, thank you for your endless wisdom and altruism. Sena, thank you for every bit of your support and encouragement, this couldn't have been done without you. Delany, thank you for your strength and belief that maintained motivation. Gerald and Otis, thank you for always being by my side.

CONTRIBUTORS AND FUNDING SOURCES

Contributors

This work was supported by a thesis committee consisting of Professor Mark Kimber and Professor Karen Vierow Kirkland of the Department of Nuclear Engineering, and Professor Maria King of the Department of Biological and Agricultural Engineering.

All work conducted for the thesis was completed by the student independently.

Funding Sources

This research made use of the resources of the High Performance Computing Center at Idaho National Laboratory, which is supported by the Office of Nuclear Energy of the U.S. Department of Energy and the Nuclear Science User Facilities under Contract No. DE-AC07-05ID14517.

NOMENCLATURE

ALWR	Advanced Light Water Reactor
AMG	Algebraic MultiGrid Solver
BC	Boundary Condition
CFD	Computational Fluid Dynamics
DNS	Direct Numerical Simulations
DOD	Department of Defense
DOE	Department of Energy
FEM	Finite Element Method
FVM	Finite Volume Method
GIF	Generation-IV Forum
HTGR	High-Temperature Gas-Cooled Reactor
HTR-10	High-Temperature Reactor - 10 MWt
INET	Institute of Nuclear Energy Technology
INL	Idaho National Laboratory
KTA	Kerntechnischer Ausschuss
MOOSE	Multiphysics Object-Oriented Simulation Environment
NGNP	Next Generation Nuclear Plant
NRC	Nuclear Regulatory Commission
NRIC	National Reactor Innovation Center
PBMR	Pebble Bed Modular Reactor
PBR	Pebble Bed Reactor
PDE	Partial Differential Equation

PIRT	Phenomena Identification and Ranking Table
R&D	Research & Development
RANS	Reynolds-Averaged Navier-Stokes
RKE	Realizable $k - \epsilon$
RPV	Reactor Pressure Vessel
SIMPLE	Semi-Implicit Method for Pressure-Linked Equations
T/H	Thermal-Hydraulic
THTR	Thorium High-Temperature Reactor
TRISO	TRi-Structural ISOtropic

TABLE OF CONTENTS

Page

LIST OF FIGURES

FIGURE Page

LIST OF TABLES

TABLE Page

1. INTRODUCTION

Initiated by the United States Department of Energy (DOE) in 2000 and sanctioned in mid-2001, the Generation-IV Forum (GIF) was first formed as a collective of 9 countries committed to joint development of a new generation of nuclear technology. GIF is the leading organization for multinational collaboration of Research and Development (R&D) for advanced nuclear energy systems and has contributed to a great deal of progress towards their goal since the signing of the GIF charter in 2001 [1]. The Generation-IV consortium aims to develop adanced reactor technology for deployment between 2020-2030 while providing significant improvements in comparison to current Advanced Light Water Reactors (ALWRs), otherwise known as Generation-III and Generation-III+ systems [2]. The most notable differences between Generation-IV reactors and previous designs consists of the offering of significant advances in sustainability, safety and reliability, economics, proliferation resistance, and physical protection [3]. With advancements of these concepts fast underway, the development of designs for commercial deployment are important for advanced reactor technology, as well as safety. One reactor of particular interest is the High-Temperature Gas-Cooled Reactor (HTGR). HTGRs are Generation-IV reactors that are considered to have revolutionary designs, however, they are not novel concepts. HTGRs have historically been under continuous development for longer than half a century, as several test reactors and prototypes have began or completed construction dating back to the United Kingdom's Dragon HTGR in 1963 [4]. Despite the lack of commercial deployment, HTGR designs continue to be a topic of interest as many prototypical designs continue to be a work in progress.

Recently, the DOE announced the National Reactor Innovation Center (NRIC) to be led by Idaho National Laboratory (INL). The NRIC is dedicated to assisting the development of advanced nuclear energy technologies, including demonstrating micro-reactor technology by developing the first micro-reactor in the early 2020s. The NRIC is also focused on demonstrating a non-LWR advanced demonstration reactor by 2030 [5], exhibiting the NRIC's advanced reactor pipeline

vision advocating for the development on advanced nuclear technology. Similarly, the United States Department of Defense (DOD) is seeking to deploy the first very Small Modular Reactor (vSMR) by the latter of 2025 for DOD installation. The purpose of the DOD deploying a vSMR displays possibilities of using this technology for employment of a mobile nuclear power plant [6] and operating independently from the electric grid to avoid vulnerability to extended power outages from various threats [7]. Several conceptual designs are currently under investigation, but design details are not publicly available. From available literature, companies such as X-energy, Urenco and HolosGen are developing potential designs based upon the Generation-IV HTGR [8]. This leads to a neccesity for continuing to characterize HTGR phenomena in the immediate future, assisting in the rapid development of various HTGR concepts due to the aggressive timeline.

HTGR designs are high-temperature, helium-cooled, graphite moderated thermal spectrum Generation-IV reactor designs. A high level of technology readiness, walk-away safety, and high coolant outlet temperatures differentiate the HTGR concepts from other Generation-IV concepts. The two common HTGR designs are the prismatic and pebble bed concepts. The prismatic core concept, is comprised of interlocking hexagonal graphite blocks with cylindrical borings that contain cylindrical fuel slugs; in the pebble bed concept the fuel is located in tennis-ball sized graphite pebbles that move through the mostly cylindrical reactor vat under gravity. Both core designs are surrounded by graphite reflector blocks. Small gaps (horizontal and axial) are required between graphite blocks in the core and reflector to avoid damage to the graphite blocks caused by thermal expansion. These gaps form secondary helium flow paths complicating the already complex thermal-hydraulic (T/H) design of these reactors. Understanding and predicting the T/H conditions within HTGRs is imperative in view of the high temperatures of fuel, graphite, and coolant on one hand, and poor heat transfer characteristics of helium on the other hand.

Due to the complexity of HTGR geometry, core coolant flow distribution is a direct function of the local core power and bypass flows, affecting core peak fuel temperatures. The flow within the HTGR traversing through the core interacts with bypass flow, resulting in the loss of 10% - 30% of expected primary flow [9]. The fraction of bypass flow, including secondary and leakage flow

paths is necessary for prediction of the core temperature distribution. Potential HTGR, SMR, and micro-reactor T/H design concerns are expected to be analogous to that of standard-sized HTGRs, but it is not fully understood which conclusions can be transferred from studies of standard-sized HTGRs. With the possibility of different aspect ratios in various HTGRs, a different core design or varied geometry, bypass flow is a phenomenon of concern due to the potential impact on T/H safety parameters.

In short, characterizing bypass flow is paramount for development of various HTGR concepts and thermal safety parameters. Characteristic to HTGRs are complex flow patterns through gaps between graphite blocks, and high coolant temperatures; during accidents flow reversal, natural circulation, and laminarization are important phenomena. Core temperature distribution is dependent on the bypass fraction, thus, excessive coolant flow within bypass gap regions can lead to violating steady-state safety margins and accident conditions. The focal point of this research will concern the HTGR pebble bed concept for bypass flow investigations, hereinafter referred to as the Pebble Bed Reactor (PBR). Due to narrow timeline development goals declared by INL's NRIC advanced reactor pipeline vision, employing Computational Fluid Dynamics (CFD) methodology is impractical due to computational costs from the aforementioned complex PBR geometry. Accelerated PBR development satisfying the NRIC timeline needs to be performed with a T/H code that can simulate full-core PBR models in a fraction of the time. T/H codes can prove to be an adequate solution for PBR development, although these lower-fidelity codes can lack the ability to account for local phenomena and important characteristics of bypass flow. This leads to a need of improving the lower-fidelity codes, which can be accomplished with the use of the computationally costly higher-fidelity Reynolds-Averaged Navier-Stokes (RANS) models. In result, improvement of a lower-fidelity code can allow for others to simulate PBR models in a cost effective manner. The primary intended contribution of the proposed research is to establish the methodology for improving closure relations in the lower-fidelity code, Pronghorn, by developing an ad-hoc approach to characterize bypass flow based on higher-fidelity RANS models. This is a critical step in establishing trusted T/H modeling for an accelerated

advancement of PBR technologies.

1.1 Objectives

To perform thermal fluid phenomena characterization analyses for a PBR, the T/H evaluation of reactor designs in the past have been based on experimental research that result in empirical correlations combined with analytic modeling [10]. Purely experimental characterization and qualification of PBRs are prohibitively expensive. This is due to experiments including detailed measurements of flow and temperature fields that are complex or not feasible. Therefore, covering the extremely large design space in detail by relying entirely on experiments is impossible. With limited experimental data and lack of experiments for PBR development, appropriate computational methods must be used for T/H analysis. Experiments are an essential portion of the design process and are indispensible for validation of computational models and confirmatory studies of promising designs, however, only promising designs should be tested via a mock-up and flawed designs should be rooted out early via computational models. By deeming experiments impractical to characterize PBR bypass flow topology, CFD provides a vital role in predicting various complex flow and heat transport characteristics. Employing CFD has plenty of practical advantages for modeling PBR fluid mechanics and heat transfer, although the complexity of the geometry and the length of anticipated transients would require an unreasonable amount of computational resources.

A two-step approach, that uses higher-order CFD methodology to parameterize a lower-resolution model, will allow for a computationally cost effective analysis of PBR bypass flow. The two-step approach can be performed by first making use of the commercial CFD software, STAR-CCM+, for higher-fidelity RANS simulations of a representative PBR model. Second, the lower-fidelity model is developed with Multiphysics Object-Oriented Simulation Environment (MOOSE), and the MOOSE-based application, Pronghorn, developed at INL. MOOSE framework enables the development of achieving complex multiphysics simulations by providing a plug-in infrastructure that simplifies definitions of physics, material properties, multiphysics coupling and postprocessing. Use of MOOSE for development of MOOSE-based

applications allows the developer to focus solely on the physics of interest without considering modern parallel computing complexities, since the MOOSE framework handles the parallel, adaptive, nonlinear, finite element solver tasks internally [11]. One MOOSE-based application that utilizes the framework is Pronghorn, a multi-dimensional coarse-mesh reactor analysis tool capable of performing T/H analyses of PBRs. Pronghorn makes use of the MOOSE framework and can perform multiscale T/H analyses of steady-state full-core PBR designs [12]. Due to the complex geometry of PBRs, multiscale techniques are a necessity for computationally efficient analyses and quick design evaluations. The complexity of the PBR designs as well as the sensitivity of bypass flow to the numerous details of the core geometry still present a difficulty for quantifying bypass flow fraction. With the use of the MOOSE framework and the capabilities available in Pronghorn, PBR simulations can be completed in a time-efficient manner, but present a need for further development of quantifying the bypass flow fraction. This provides motivation for numerical modeling by utilizing higher-fidelity CFD methodology to characterize PBR bypass flow phenomena. By developing a model with a smaller domain that maintains the inherent characteristics of a PBR, an efficient dataset can be produced with CFD and parameterized to provide an ad-hoc approach quantifying bypass flow for the lower-fidelity T/H core simulator. The development of an accurate ad-hoc approach s can then be implemented into Pronghorn for characterization of PBR bypass flow for several parameter consideration. In result, this higher-order numerical analysis will allow for rapid PBR development as the ability to simulate full-core models becomes computationally cost efficient and can provide results in a fraction of the time. **The contribution of this research is the first demonstration of bypass flow predictive tools in Pronghorn, informed from flow physics extracted from CFD.** This contribution is realized through the following research tasks:

I. Conduct CFD simulations within STAR-CCM+ covering range of operating conditions and bypass flow geometry;

II. Develop pressure loss correlations from CFD data and implement algorithm in Pronghorn to compute bypass flow distribution;

III. Demonstrate efficacy of algorithm by comparing a test case from Pronghorn to results from additional CFD dataset.

2. STATE OF THE ART

2.1 Pebble Bed Reactors

HTGR Research & Development (R&D) has developed an array of potential designs, nonetheless, they all are equipped with the same basic features and performance attributes. The basis of all the designs revolves around a high-temperature, helium-cooled, graphite moderated thermal spectrum. The defining characteristic of a PBR, however, is the randomly packed core with spherical fuel elements, otherwise known as pebbles. PBR pebbles are TRi-structural ISOtropic (TRISO) coated fuel particles that consist of three layers of pyrolytic carbon and one layer of silicon carbide [13]. PBRs for power generation are envisaged to utilize a multi-pass continuous refueling scheme where fuel pebbles are continuously loaded and traverses through the core with gravity. The pebbles are evaluated upon exiting the discharge tube, and can be reinserted multiple times if the target burnup is not exceeded. For example, the High-Temperature Reactor - 10 MWt (HTR-10) can reinsert the TRISO fuel spheres roughly 5 times before disposing of the pebble [14]. The arrangement and process of the multi-pass refueling scheme can be seen in the general PBR schematic in Fig. (2.1).

Helium serves as the coolant for the PBR. Helium is an inert gas that does not chemically react with other materials in the reactor core and is unaffected by neutron activation, resulting in good neutron economy. Helium primarily travels through an open plenum above the pebble bed and down the reactor core, passing through the pebble bed by interconnected voids between the pebbles to remove fission heat. Helium removes heat from the core, consequently heating up and moving to a power conversion system that generates electricity. Other notable PBR components include the reactor internals, which consist of graphite materials. The graphite serves as both the neutron reflector and for thermal insulation, forming the ceramic internals that contain the active core fuel elements. Surrounding the pebble bed is the graphite moderator or reflector in the form of numerous loosely-stacked graphite blocks. Helium is able to exit the pebble bed through the

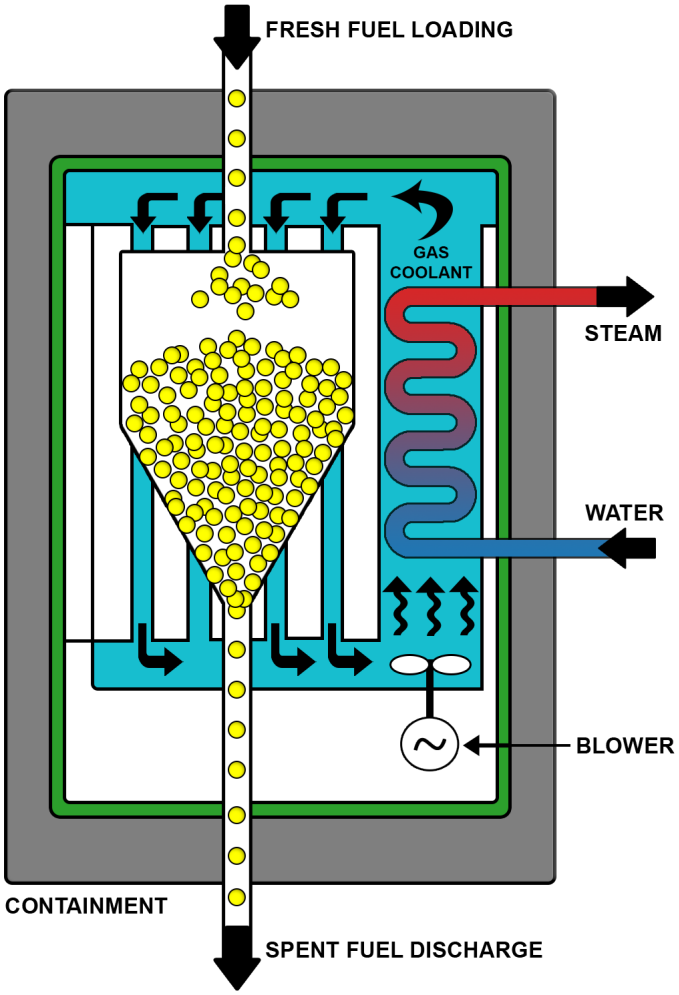

Figure 2.1: General PBR schematic

bottom reflector, which has numerous machined holes that link the reactor core to the hot legs, or hot coolant flow paths to the steam generator.

With some of the important PBR features reviewed, the HTR-10 will be covered as the reference PBR for domain considerations and future discussion. The HTR-10 components and geometry will be summarized to gain a greater understanding of the helium flow paths.

2.2 HTR-10 General Description

Designed and constructed by the Institute of Nuclear Energy Technology (INET) of Tsinghua University in China, the HTR-10 is a 10 MWt test reactor that represents a general PBR design with

similar features and inherent safety characteristics [14]. The reactor consists of a Reactor Pressure Vessel (RPV), internal graphite structures, TRISO fuel elements, control rods, a small absorber ball shut-down system, as well as other components. The main design parameters of the HTR-10 are tabulated in Table (2.1). Fueled by TRISO fuel, the HTR-10 has the capability to achieve high coolant temperatures as well as high fuel burnup levels [15]. Roughly 27,000 randomly packed TRISO spheres, or pebbles, are placed in the core and encompassed by graphite blocks. The HTR-10 core is a cylindrical cavity positioned above a conical zone known as the 'conus', which funnels the pebbles into the discharge tube. As the pebbles approach the discharge tube, the helium exits the reactor core through numerous borated holes in the graphite. The HTR-10 is cooled by helium gas and reflected by numerous stacks of graphite blocks, analogous to the general PBR design aforementioned in Section (2.1).

Table 2.1: Primary HTR-10 design parameters

Parameter	**Value**
Reactor Thermal Power (MWt)	10.0
Primary Helium Pressure (MPa)	3.00
Reactor Core Diameter (cm)	180
Reactor Average Core Height (cm)	197
Average Helium Temperature at Reactor Inlet (°C)	250
Average Helium Temperature at Reactor Outlet (°C)	700
Helium Mass Flow Rate at Full Power (kg/s)	4.32
Average Core Power Density (MW/m^3)	2.00
Power Peaking Factor (PPF)	1.54
Fuel Type	TRISO - UO_2

Beyond the primary flow path where helium traverses through the pebble bed, alternative flow paths exist due to the complexity of the geometry. The flow path classifications in a PBR include primary, secondary, leakage and bypass flow paths. Secondary flow is the engineered flow paths that cool key components in the reflectors, such as the control rods. Leakage flow occurs through

engineered components, essentially the small absorbing sphere and control rod channels, where sleeves are positioned between each block that result in small leakage gaps. Bypass flow includes the secondary and leakage flow paths, as well as any flow that bypasses the pebble bed completely. Bypass flow most notably considers flow paths between the graphite blocks. Designed for safety considerations, the HTR-10 has numerous stacks of graphite blocks that form a loose body structure with narrow gaps to account for thermal expansion. Large thermal stresses can lead to brittle fracture of the graphite blocks that are too large or in contact, hence, the gaps are designed to avoid these concerns with said gaps between each block. These gaps can also deform or expand due to thermal- and irradiation-induced deformation. Presence of gaps between graphite blocks introduces the possibility of a percentage of helium flow from the primary flow path and entering into gaps between each graphite block. The bypass flow between the graphite blocks can cause insufficient coolant flow through the pebble bed, resulting in increased temperature distributions within the core, raising thermal safety concerns. Previous literature has reported for every 1% increase of bypass flow, maximum temperature of the coolant, fuel surface and center will increase by 7 °C [16]. Therefore, bypass flow phenomena are key to safety analysis in a PBR, but the flow patterns remain difficult to determine due to small height/width ratios [17]. Consideration of both vertical and horizontal flow in the HTR-10 reflectors is necessary, and the HTR-10 loose body structure of graphite blocks is formed by every block connected to its neighbors with dowels and keys, further complicating the geometry of the bypass flow paths. For simplification, the blocks interlocking mechanisms are neglected. As shown in Fig. (2.2), the vertical and horizontal gaps are evaluated without keys, dowels, or the possibility of deformation.

To conclude, the HTR-10 described in this section is designed with key components built into graphite blocks, including 10 control rod guide channels, 7 shutdown absorber ball channels, 3 experimental channels, and 20 cold gas channels. These channels are engineered into the structural components via borated holes. A two-dimensional radial cross-section of the HTR-10 is adapted from [18] and provided in Fig. (2.3) for further clarity.

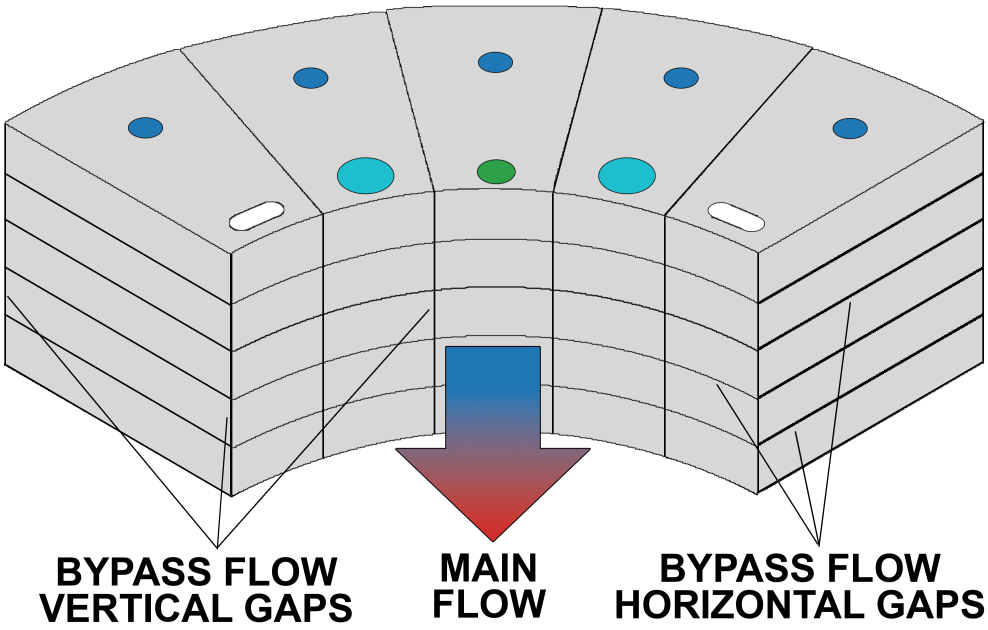

Figure 2.2: Vertical and horizontal (circumferential) bypass gaps between graphite blocks

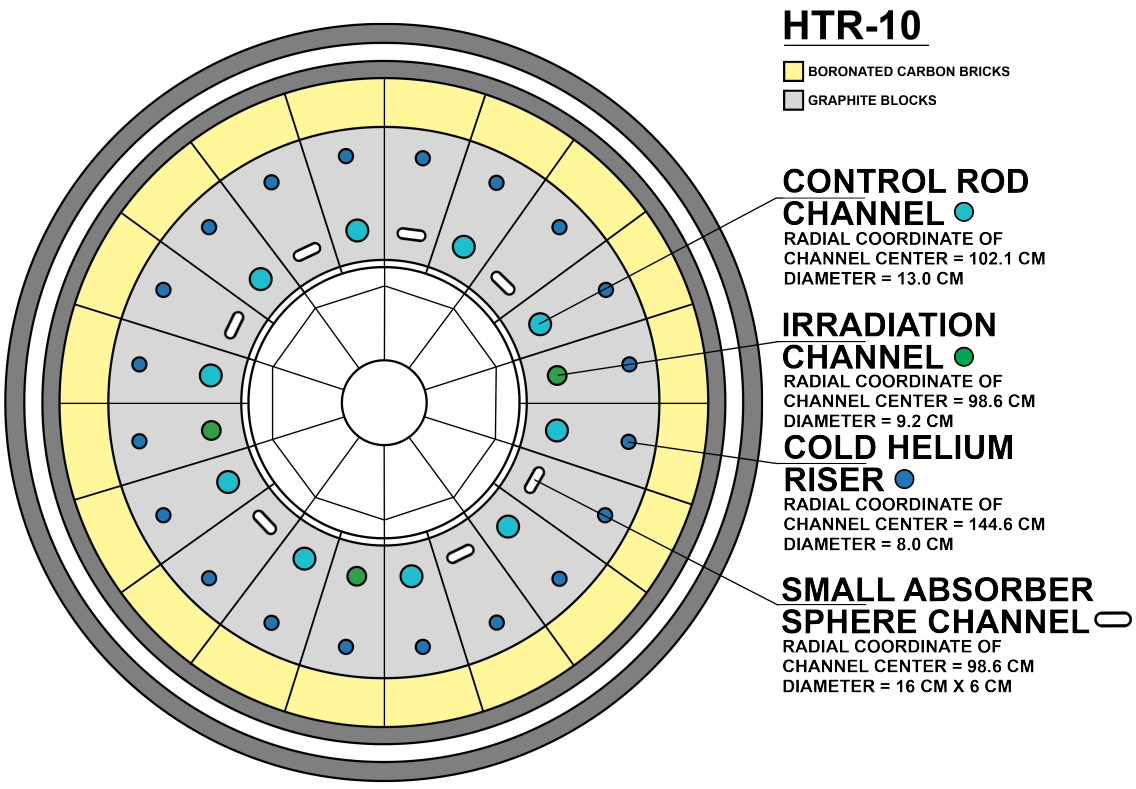

Figure 2.3: HTR-10 two-dimensional radial cross-section with identified key components adapted from [18].

2.3 Research Motivation

As introduced in Chapter (1), the complexity of PBR geometry results in core coolant flow distribution as a direct function of the local core power and bypass flows, affecting core peak fuel temperatures. Due to the potential of core peak temperatures rising from excess bypass flow, incidents pertaining to insufficient cooling of the fuel raise T/H safety concerns for the phenomenon. Concerns regarding bypass flow phenomena continue beyond the excess bypass flow event described, raising the need to investigate underlying difficulties that are present to even infer the amount present in the system. In typical PBR designs, bypass flow does not serve solely as a demerit to the system since it benefits in several ways such as removing heat from the pebble bed to the side reflector. This further complicates the concerns of the phenomenon since common PBR designs can't eliminate bypass flow entirely, and the appropriate resolution is a continuation of performing studies for the purpose of gaining a greater understanding of bypass flow in the PBR.

Determining that the importance of information for certain analyses needs to be classified as a higher priority than other areas under consideration is common in the nuclear industry today. Identifying areas in need of assessment by importance is commonly performed with a Phenomena Identification and Ranking Table (PIRT) process, where information is gathered systematically from subject matter experts on the specific concept. The PIRT process has been demonstrated to be successful to numerous technology issues dating back to the development of the PIRT in the late 1980s [19]. PIRT processes have been beneficial to the analyses, by guiding research or developing requirements, so it is no surprise that a refined generalized process was determined a decade later for nuclear applications [20]. PIRT exercises are still conducted presently, including sponsored studies by the Nuclear Regulatory Commission (NRC) to assist in developing or refining NRC guidelines.

One of the PIRT exercises of interest was conducted considering Next Generation Nuclear Plant (NGNP) designs and published in 2008 by the NRC [21]. In this exercise, five panels of subject matter experts identified and ranked phenomena critical to steady state and accident

conditions. One panel in particular was tasked with discussing accident and T/H analysis (including neutronics) for various designs of the prismatic reactor and PBR. Resulting from the PIRT exercise, safety-relevant NGNP phenomena were identified and ranked for areas of concern considering normal operation and postulated accident conditions. These designs did not consider TRISO fuel for the PBR, however, the study can be deemed a success compared to a similar effort attempted in a PIRT exercise considering PBRs with TRISO fuel in 2004. The TRISO fuel study does not hold as high regard as it was appreciably more general since the panel stated a lack of specifics were given to develop a more detailed approach [22]. Each safety-relevant phenomena identified from the 2008 PIRT exercise were assigned with an importance rank of either high, medium, or low along with rationale. A high importance rank is defined for phenomena that have a controlling influence on the primary evaluation criterion. The rationale provided consists of a Figure of Merit (FOM) in relation to one or more evaluation criterion. Following importance rankings, panel members ranked the current knowledge level of the phenomena in the PIRT tables with the same notation as importance; defined by high, medium, or low based on a reflection of the knowledge levels, competency of available analytical tools and data. The resulting tables considered bypass flow during normal operation (20% - 100% power) to have high importance with a low knowledge level, advising further study since it was determined that the flow is either extremely difficult or impossible to measure.

PIRT exercises employed for NGNP designs such as the PBR provide confirmation that characterization of bypass flow should be a priority when developing nuclear reactor designs and technology due to the lack of knowledge, analytical tools and data available at the current time of publication. The rationale provided in the report still holds true today that many challenges arise when attempting to predict and/or model bypass flow. For instance, quantifying bypass flow between the graphite blocks presents challenges, yet over the period of operation in the PBR, the graphite blocks also experience deformation from stress that is induced from thermal and radiation effects. The variation of shape that the graphite blocks experience only increase the difficulty in accurately computing the bypass flow in the system. With the graphite blocks shape

altering from the aforementioned effects, there are changes in the fluid flow paths present in the bypass region, which results in a variation of bypass flow in the axial direction along the core [23]. Nevertheless, the PIRT exercise served purpose as intended. Since the study was originally published in 2008, the majority of reported factors that influence bypass flow have already been investigated or are under investigation to the present day.

Although numerous studies have been conducted with respect to bypass flow, this phenomenon still has a number of factors yet to be determined. In addition to further investigations needed to characterize bypass flow, the recent strong motivations displayed in support for developing Generation-IV reactors and advanced nuclear technology is not possible without indisputable evidence that bypass flow is accounted for and not a concern in any potential PBR design. A greater motivation for this research arises not only from insufficient knowledge of PBR bypass flow, but in addition, deeming a need to have the capability to assess this phenomenon in a rapid and efficient manner. As mentioned in the introduction to this bypass flow investigation, utilizing a two-step approach with the use of RANS is necessary to acquire an adequate dataset of parameters that have relation to bypass flow. Extensive computational resources are required to attain the dataset, demonstrating the need for a computational tool that requires an appropriate computational expense for simulating PBR systems, including bypass flow. While it is imperative to characterize bypass flows in a PBR, an optimistic inclination to progress efforts towards capabilties of computationally efficient analyses for the purpose of rapid design evaluations serves as motivation.

3. CFD BYPASS FLOW INVESTIGATION

Bypass flow investigations using CFD are conducted with Simcenter STAR-CCM+, a commercial CFD based simulation software. STAR-CCM+ has the ability to model and analyze a broad range of engineering problems including single- and multi-phase flow, heat transfer, solid mechanics, electromagnetics among other phenomena of interest. This investigation employs STAR-CCM+ 2020.3 (v. 15.06.008-R8) unless otherwise noted.

3.1 Computational Methodology

Development of a computational domain representative of the PBR is essential to analyze the bypass flow phenomenon. While modeling the PBR entirely can provide a computational domain comparable to existing reactor designs, extensive computational resources are required. An appropriate computational domain for this study is based on the HTR-10 discussed in Section (2.2) with several assumptions to reduce the computational expense accordingly. First, the graphite blocks in the reflectors surrounding the PBR core are modeled without the presence of key components such as the control rods or small absorber sphere channels. Second, the graphite blocks neglect the dowel and dowel socket system that connect the blocks vertically in addition to the key and keyway system connecting the blocks horizontally in the core structure of the HTR-10 [24]. Furthermore, the graphite blocks are modeled with the assumption that thermal- and irradiation-induced deformation does not occur, similar to [25]. It is also assumed the bypass gaps modeled both horizontally and vertically have uniform thickness.

Several investigations of bypass flow phenomena utilize detailed computational domains for prismatic HTGR [26, 27] and PBR concepts [28, 29, 30]. Reducing the computational cost for bypass flow investigations has been performed by building a flow network to account for flow distribution in the PBR, only using CFD for small areas of interest where parameters are unknown [31, 32, 33, 34, 35]. The representative PBR model and assumptions this study entails is most similar to [36], consisting of a HTR-PM bypass investigation using CFD for a large percentage

of the domain to capture important phenomena. All studies aforementioned in this section have discussed the presence of bypass flow gaps that vary in thickness from 0.1 mm - 6.0 mm.

Additional simplifications are also applied to the representative PBR to reduce the overall size of the domain. As previously discussed, the HTR-10 core funnels the pebbles into a conus, allowing for the removal of the hot gas coolant. Numerous details are required for modeling the conus, such as the dozens of borated holes and the angled graphite structures, however, only the reactor core and cavity above the core is considered. This reduces the size of the computational domain as well as detailed development of the conus domain. By modeling only the PBR cavity and pebble bed, this also results in the consideration of 19 of the 20 bypass gaps, characteristic to the HTR-10. A final assumption for simplifying the PBR computational domain is modeling a two-dimensional axisymmetric geometry, a representative slice of the actual three-dimensional model revolved around an axis. The computational domain is shown in Fig. (3.1), where the porous media and the fluid flow paths are considered.

To further discuss the PBR computational domain, prior to entering the reactor core, the coolant typically travels through an open area above the randomly packed pebbles. This area is referred to as the cavity, which consists solely of helium fluid flowing down to the pebble bed or possibly shifting to the bypass gaps. Within the reactor core, the HTR-10 has a reported packing fraction of 0.61, and the pebble bed interacts with gaps 7-19 downstream from the cavity. In Fig. (3.1), the graphite blocks and carbon bricks noted are considered for the computational domain, but the solid modeling is not. The modeled PBR domain only considers porous media and fluid flow by simplification, resulting in the absence of conjugate heat transfer in the side reflectors. The gaps are a constant thickness, $\delta = 1, 2, 3$ mm, modeled with the same gap size throughout as well. This means that the vertical gap that interconnects the outer layer of carbon bricks with the inner layer of the graphite blocks will always be the same width as the gaps.

A mesh tool is utilized with STAR-CCM+ for discretization of the domain. Using the directed mesh tool available, a structured mesh is created for the PBR. Direct meshing is ideal for meshing finite volume fluid flow simulations since it supplies a structured mesh in the axial direction. A

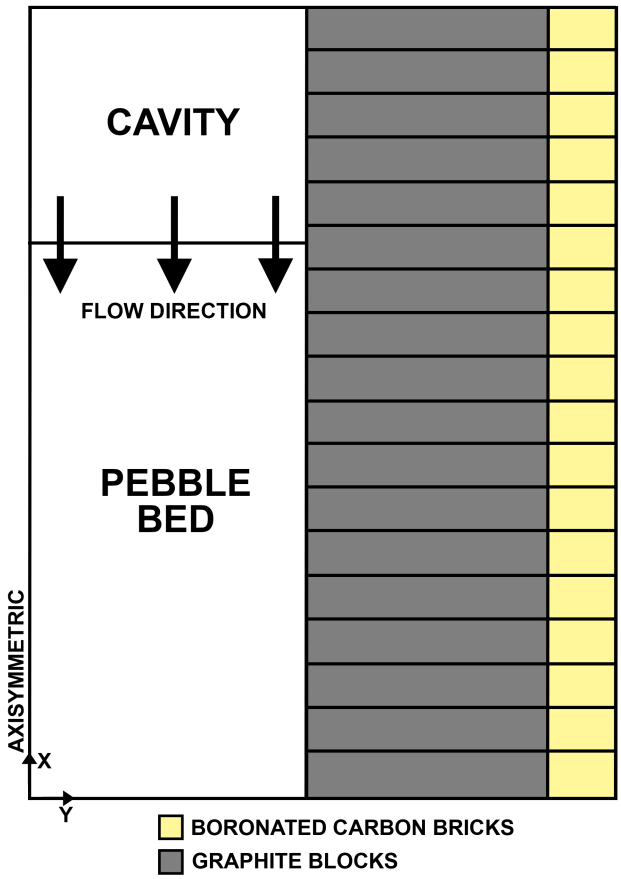

Figure 3.1: Two-dimensional axis of revolution STAR-CCM+ model of PBR

coarse, medium, and fine mesh were created for 1 mm, 2 mm, and 3 mm gaps, respectively. The structured mesh presented in Fig. (3.2) is obtained from the 3 mm gap model, where it should be noted that the domain is rotated 90 degrees compared to Fig. (3.1). The STAR-CCM+ model is rotated 90 degrees since the x-axis is required to be the axis of rotation. For the coarse, medium and fine mesh the computational domain is discretized into 372,750 cells, 1,491,200 cells, and 5,964,000 cells. The wall spacing is defined as 1E-06 m to capture the phenomena in the gaps due to their small size, which can be seen by the red and blue highlighted subfigures in Fig. (3.2). The blue box shows the refined mesh in the gaps near the cavity and pebble bed, while the red box shows the refinement where the first and second section of horizontal gaps connect with the vertical gap. The y^+ value is maintained between $1 < y^+ < 30$ with an all-y^+ wall treatment, which is recommended when it is difficult to achieve a pure high-y+ or low-y+ mesh because of varying

geometrical and velocity scales associated with the model.

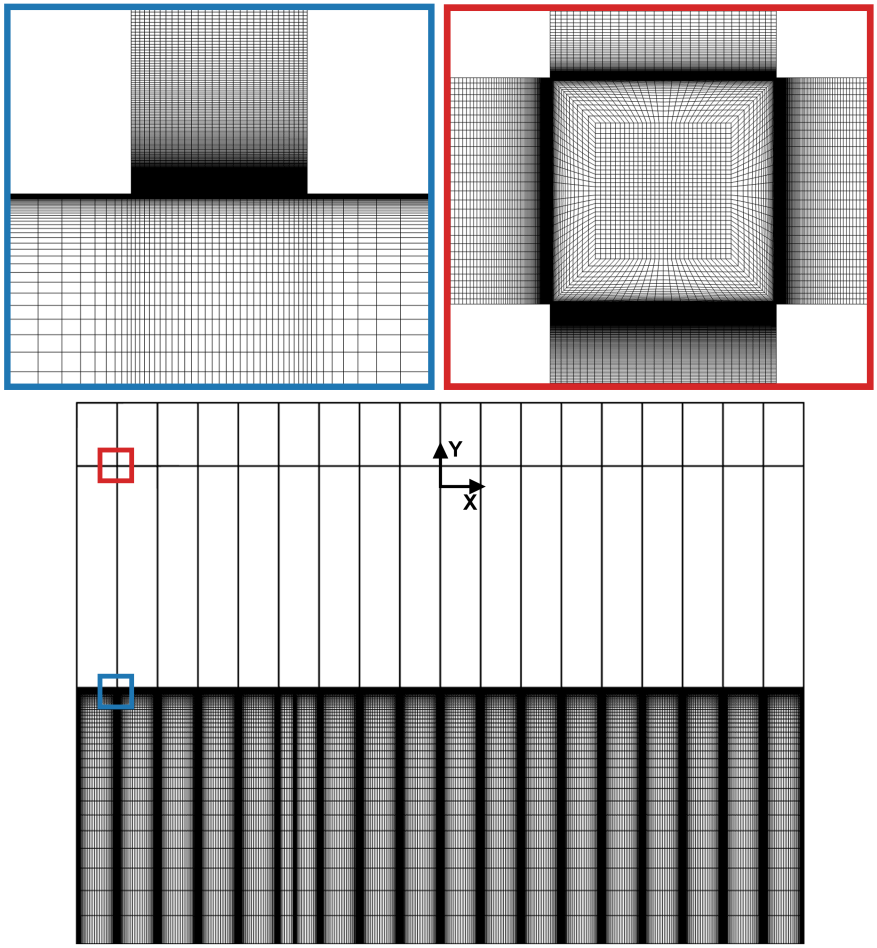

Figure 3.2: Medium density computational grid for $\delta = 3\ mm$ two-dimensional axisymmetric PBR

3.2 Governing Equations

Modeling physics phenomena is founded on derivations from fundamental laws that exhibit conservation principles. STAR-CCM+ exercises mathematical principles on a macroscopic scale, modeling materials as continua and characterizing physics derived from fundamental laws that demonstrate conservation principles. A Eulerian or control volume approach is adopted considering a volume of space where material flows, allowing conservation laws for a continuum

to be expressed. Conservation laws are fundamental principles that govern the total property considered so that it remains unchanged during the physical process. With respect to continuum mechanics, three conservation laws govern the mechanics of fluids; (1) conservation of mass, (2) conservation of linear momentum, and (3) conservation of energy. Continuum mechanics conservation laws are presented in differential form for an infinitesimal control volume. Conservation of mass is defined as a mass balance through a control volume, or continuity equation by,

$$\frac{\partial \rho}{\partial t} + \nabla \cdot (\rho v) = 0 \tag{3.1}$$

where ρ is density, and v is velocity in the continuum. Conservation of linear momentum can be expressed by,

$$\frac{\partial}{\partial t}(\rho v) + \nabla \cdot (\rho v \otimes v) = \nabla \cdot \boldsymbol{\sigma} = -\nabla \cdot (p\mathbf{I}) + \nabla \cdot \mathbf{T} \tag{3.2}$$

where $\boldsymbol{\sigma}$ is a stress tensor. Stress tensors for fluids consist of the sum of normal and shear stresses, where $\mathbf{I}$ is the identity tensor, $\mathbf{T}$ is the viscous stress tensor, and p is the pressure. The concept of this conservation law considers linear momentum with respect to the time, where the rate of change is equal to an acting force on the continuum. Conservation of energy utilizes the first law of thermodynamics applied to a control volume, formulated by,

$$\frac{\partial(\rho E)}{\partial t} + \nabla \cdot (\rho E v) = \nabla \cdot (v \cdot \boldsymbol{\sigma}) - \nabla \cdot q + S_E \tag{3.3}$$

where E represents total energy per unit mass, heat flux is specified as q, and an energy source per unit volume is designated by S_E.

PBR physics are evaluated for fluid flow and heat transfer via the conservation equations designated in Eqs. (3.1-3.3). Computing applicable phenomena that represent appropriate PBR physics in this study consider the presence of turbulent flow approximated by a turbulence model.

3.2.1 Turbulence

Due to the turbulent flow present in the large size of the HTR-10 domain, the most practical application of turbulence modeling is employing the Reynolds-Averaged Navier-Stokes (RANS) equations. RANS-based turbulence models are routinely used in many engineering disciplines as they provide a great deal of convenience and computational efficiency. Turbulent flow simulations that implement RANS-based turbulence models reduce computational costs with closure relations implemented to govern the transport of mean flow properties. Formulation of the RANS equations for mean quantities involves temporal averaging for the steady-state simulations conducted. The construction of the RANS equations is detailed below by first decomposing an instantaneous solution variable of interest into the sum of the mean and fluctuating components,

$$\phi = \overline{\phi} + \phi' \tag{3.4}$$

where ϕ can represent field components such as velocity, pressure, or energy within the system. The mean or averaged value is termed as $\overline{\phi}$ and the fluctuating component is ϕ'. Applying this process to the governing equations defined by Eqs. (3.1-3.3), RANS expressions for conservation of mass, linear momentum, and energy are obtained, respectively. The RANS equations are defined below as,

$$\frac{\partial \rho}{\partial t} + \nabla \cdot (\rho \overline{v}) = 0 \tag{3.5}$$

$$\frac{\partial}{\partial t}(\rho \overline{v}) + \nabla \cdot (\rho \overline{v} \times \overline{v}) = -\nabla \overline{p} + \nabla \cdot [\mathbf{T} + \mathbf{R}_{RANS}] \tag{3.6}$$

$$\frac{\partial}{\partial t}(\rho \overline{E}) = \nabla \cdot (\rho \overline{v} E) = \nabla \cdot [(\lambda + \lambda_{RANS}) \nabla \overline{T}] + \overline{v} \cdot (\mathbf{T} + \mathbf{R}_{RANS}) \tag{3.7}$$

The resulting RANS equations regarding mean quantities are almost identical to the aforementioned fundamental conservation equations of fluid flow and heat transfer. A distinction

can be made between the non-RANS equations defined as Eqs. (3.1-3.3) and RANS equations shown as Eqs. (3.5-3.7) with the addition of two terms on the right-hand side of the expressions for momentum and energy. The RANS momentum transport displayed in Eq. (3.6) introduces the divergence of a second-order tensor, $\mathbf{R}_{RANS}$, the Reynolds stress tensor. The energy transport equation shown as Eq. (3.7), includes an addition of the Reynolds stress tensor, as well as turbulent thermal conductivity, λ_{RANS}. These two key additional terms specify interactions between turbulent fluctuations in the RANS transport equations.

Determining an appropriate turbulence model is dependent on the desired level of accuracy and computational expense. Consequently, common practice utilizes RANS turbulence models due to reasonable computational cost and resulting accuracy. The most widely used RANS turbulence models are the two-equation $k-\epsilon$ and $k-\omega$ models. Both of these turbulence models present additional transport equations that must be solved in conjunction with the RANS equations to complete closure. Both two-equation models solve for turbulent kinetic energy, k, as well as respectively solving for either turbulent dissipation rate, ϵ, or specific dissipation rate, ω. The additional turbulence quantities that are computed with the two additional transport equations allow for a complete description of the turbulence, allowing for effects of transport of turbulence properties [37]. The $k-\epsilon$ model first developed by [38] is of interest moving forward, due to the applicability for HTGR flow regimes. The general forms for the $k-\epsilon$ transport equations are shown in Eq. (3.8) for turbulent kinetic energy and Eq. (3.9) for turbulent dissipation rate below.

$$\frac{\partial}{\partial t}\Big(\rho k\Big) + \nabla\cdot(\rho k\overline{v}) = \nabla\cdot\left[\left(\mu+\frac{\mu_t}{\sigma_k}\right)\nabla k\right] + P_k - \rho\epsilon \tag{3.8}$$

$$\frac{\partial}{\partial t}\Big(\rho\epsilon\Big) + \nabla\cdot(\rho\epsilon\overline{v}) = \nabla\cdot\left[\left(\mu+\frac{\mu_t}{\sigma_\epsilon}\right)\nabla\epsilon\right] + \frac{\epsilon}{k}C_{\epsilon1}P_\epsilon - C_{\epsilon2}\rho\frac{\epsilon^2}{k} \tag{3.9}$$

In the expressions for turbulent kinetic energy and turbulent dissipation above it should be noted that $\overline{v}$ is the mean velocity, μ is the dynamic viscosity, k is the turbulent kinetic energy, and ϵ is the turbulent dissipation rate. The equations above contain variables σ_k, σ_ϵ, $C_{\epsilon1}$, and $C_{\epsilon2}$, defined as model coefficients dependent on the $k-\epsilon$ model variant. The production term P_k is the production

of turbulence due to shear, representing the generation of turbulent kinetic energy due to the mean velocity gradients. The second production term, P_ϵ, is the production of turbulent dissipation by strain rate. Production terms are formulated depending on the $k-\epsilon$ model variant.

Considering the complex flow topology present in PBR designs such as the HTR-10, the standard $k-\epsilon$ model is adequate for use, however an alternative two-equation $k-\epsilon$ model is presented due to the substantial improvement for this particular application. The Two-Layer Realizable $k-\epsilon$ (RKE) model developed by [39] is a variant of the standard $k-\epsilon$ model that provides greater capabilties to solve a variety of complex flows, including strong adverse pressure gradients, flow separation and recirculation. Additionally, the Two-Layer RKE model calculates eddy viscosity without a constant value of C_μ, expressing the coefficient as a function of mean flow and turbulence properties. The function to determine C_μ arises in the Two-Layer RKE model due to non-linear constitutive relations present, requiring the variable coefficient to be quantified by,

$$C_\mu = \frac{1}{4+\sqrt{6(S:S+W:W)}\cos\xi} \tag{3.10}$$

where S is the strain rate and W defines the vorticity tensors. In addition, turbulence model constants for the Two-Layer RKE model are tabulated in Table (3.1).

Table 3.1: Two-Layer Realizable $k-\epsilon$ model closure coefficients

$C_{\epsilon 1}$	$C_{\epsilon 2}$	σ_k	σ_ϵ	ξ
$max\left(0.43, \frac{\eta}{5+\eta}\right)$	1.9	1.0	1.2	$\frac{1}{3}\arccos\left(\frac{S\cdot S\cdot S}{\sqrt[3]{S:S}}\right)$

Due to the complexity of the flow field, the RKE model is used analogous to previous studies [40, 41, 42]. In addition, the two-layer approach was employed for an all-y$^+$ wall treatment. The two-layer RKE model is standard in the commercial CFD package, STAR-CCM+, combining a two-layer approach with the RKE model, adding the ability of using the aforementioned all-y$^+$

wall treatment. The Two-Layer RKE model offers the most mesh flexibility and produces the least inaccuracies for intermediate meshes, particularly $1 < y^+ < 30$ [43]. All simulations were performed with the Two-Layer RKE turbulence model.

3.3 Computational Procedure

Using the segregated flow solver, STAR-CCM+ utilizes the finite volume method (FVM) for discretization of the Navier-Stokes equation that iteratively quantifies the flow field with the Semi-Implicit Method for Pressure-Linked Equations, or SIMPLE algorithm. The SIMPLE algorithm resolves pressure-velocity coupling of the Navier-Stokes equations [44] with the Rhie and Chow method [45] used for interpolating flux at the cell faces. Within the segregated flow properties, a 2nd-order upwind discretization scheme is selected for computing the convection term in the appropriate governing equations. With the use of the Algebraic MultiGrid Solver (AMG) approach, a highly efficient and robust system of linear solvers is built to solve the governing equations iteratively [46]. The segregated solver algorithm is replicated until the normalized residuals for all relevant equations reduce to values lower than 1E-6. This normalized residual criterion has been proven in previous studies to be sufficient for tight convergence of all relevant quantities [47]. A summary of the solver settings and discretization schemes are presented in Table (3.2). In order to stabilize simulations and achieve a converged solution, the under-relaxation factors are adjusted accordingly. Considering steady state simulations for porous media, it is recommended to decrease the under-relaxation factor for velocity to 0.5 and the pressure under-relaxation factor to 0.1 [43].

Table 3.2: Summary of finite-volume simulation and discretization settings

Simulation Setting	**Selection**
Solver	Segregated
Pressure-Velocity Coupling	SIMPLE
Turbulence Model	Two-Layer Realizable $k - \epsilon$
Momentum Discretization	Second-Order Upwind
Energy Discretization	Second-Order Upwind
Turbulence Discretization	Second-Order Upwind

Helium fluid material properties are considered in a continued effort to model the PBR closely to the HTR-10. Implementation of the helium properties can be performed by defining each correlation in a user-defined field function in STAR-CCM+. Helium material property correlations are utilized from previous literature [48] that covers a vast range for both temperature and pressure (293 K to 1773 K, 1 to 100 bar) With such a wide scope of applicability, the equations to calculate for helium properties are ideal for a PBR and would not be a concern regarding the range. The helium correlations have been adopted by the German Nuclear Safety Standards Commission, Kerntechnischer Ausschuss (KTA). KTA is tasked with issuing nuclear safety standards for various topics that focus on nuclear technology. HTGR core design considerations are published as the set of standards as Safety Standard KTA 3102, with efforts focused on reactor core design for HTGRs. Safety Standard KTA 3102 includes adopting the helium correlatiosn discussed for Safety Standard KTA 3102.1 [49]. Material property correlations for helium are tabulated in Appendix (A), where STAR-CCM+ quantifies density with reference to Safety Standards KTA 3102.1 using Eq. (A.1).

3.3.1 Porous Media Modeling

With the properties for turbulence and helium defined, the most significant portion of the model must be considered, porous media. Fluid flow through the pebble bed is considered by the transport of fluid or energy through porous media. The PBR core generally consists of thousands of randomly packed fuel pebbles that are sufficiently cooled by fluid flow through interstitial flow paths or effective pore space to form a porous media continuum between the pebbles [50]. This region is the porous medium, or a portion of space occupied by multi-phase matter. Modeling the porous structure in detail would require extensive computational resources, therefore STAR-CCM+ employs an alternative approach by approximating porous media using appropriate loss coefficients. STAR-CCM+ characterizes a porous medium in two different ways, porous region modeling and porous media modeling. Each porous media model approach considers different characteristic length scales for velocity and the presence of heat transfer. Porous region models are common in comparable computational tools such as ANSYS FLUENT [51], but

neglect solving for a separate solid energy equation resulting in the fluid and solid calculated as the same temperature. Porous region modeling is sufficient in many practices, however, it is not representative of nuclear reactors, leading to unsuitable analyses in the past [52]. Typical to the PBR, the porous media model is utilized accordingly to account for heat transfer between the two phases in the porous medium.

In addition, the porous media model in STAR-CCM+ approximates the porous media with loss coefficients. Inertial and viscous resistance values were defined for the porous medium by employing user-defined functions with Eq. (A.13a) and Eq. (A.13b) accordingly. Resistance for both the inertial and viscous term applied correspond to the KTA drag model presented in Appendix (A.2.2) that are obtained from KTA safety standards [53]. Analogous to defining helium properties, solid graphite properties are accounted for in porous media based on applicable correlations representative of a general PBR. Thermal conductivity of the solid is implemented as a user-defined function considering the Breitbach and Bartels correlation [54],

$$k_s = 1.1538 \cdot 10^{-6}(T + 100)^{1.6622} \tag{3.11}$$

where the thermal conductivity of a uniform pebble bed must be quantified at temperatures above 250 $^{\circ}\mathrm{C}$ and k_s is the solid thermal conductivity. For solid thermal conductivity all the relevant heat transfer mechanisms in the pebble bed are defined as a single representative conduction process [55]. Density and specific heat also are defined for porous media with reference to previous literature for recommended material preoperties of the German graphite fuel pebble for the HTR-10 [56]. With the computational methodology established, including turbulence modeling and porous media modeling, attention is made on efforts that can loosely be described as validation of the CFD results, making use of semi-analytical modeling to ensure expected trends are captured.

4. FIRST PRINCIPLE ANALYSIS

4.1 Model Methodology

In an effort to demonstrate the feasibility of the respective PBR model results generated using CFD, a first principle analysis is conducted by considering the representative PBR and solving for the bypass gap mass flow rates for comparison. To perform the analysis and find a solution for the bypass flow, the domain modeled the computational domain in STAR-CCM+. With this approach, the PBR cavity and pebble bed are considered with 19 bypass gaps adjacent to the core, in the PBR side reflector region. The mathematical formulation of this effort is achieved by considering each unique flow path through the reactor and bypass gaps and recognizing that the overall pressure drop from initial entry to final exit must be the same, regardless of the path taken between those two points. There are a total of 19 unique flow paths, the first six of which are illustrated in Fig. (4.1). Of course, there are 19 unknown mass flow rates representing the flow departing from the cavity or pebble bed region into the bypass flow region. Taking the overall mass flow rate to be a known quantity, the final unknown is the overall pressure drop. The challenge then is to sum up the pressure drop components for each path and set each of those 19 equations equal to the overall pressure drop. The final equation to establish a well-defined mathematical formulation of 20 equations and 20 unknowns is the sum of all the individual mass flow rates (the 19 mass flow rates through the bypass gaps plus the residual that exits at the bottom of the pebble bed) must yield the overall mass flow rate. It should be noted that the CFD domain also includes the boronated carbon bricks which would introduce an additional 19 unknowns. For this exercise, those bricks are neglected since the primary purpose of this analytical model is to strengthen the confidence placed in the CFD results, not to fully validate those results.

To elaborate on the first principle analysis summarized above, several considerations are made. To compute the 20 unknown values, the pressure drop in each respective region must be summed to calculate an overall pressure drop. Considering the representative PBR, a function is defined

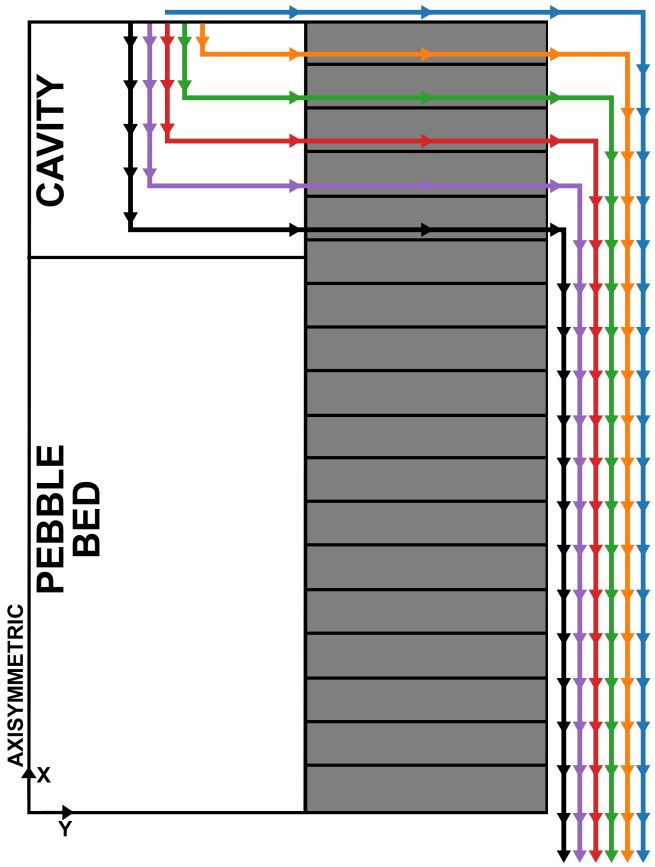

Figure 4.1: Simplified diagram of the fluid flow paths considered for first principle analysis

that quantifies the pressure loss in each flow path by,

$$f(x) = \begin{cases} \Delta P_{core} & where\ N = 19 \\ \Delta P_{gap,N}, \quad for\ i = 1, \cdots, N, \end{cases} \tag{4.1}$$

where N is defined as the number of bypass flow gaps and ΔP is the pressure loss. Loss in the cavity is computed with the use of the Darcy-Weisbach equation, which relates the head loss or pressure loss due to fluid friction assuming fully developed, steady, incompressible flow [57]. The pressure loss form of the Darcy-Weisbach equation can be written in terms of velocity or mass flow

rate as,

$$\Delta P = f \cdot \frac{\rho V^2}{2D} \cdot L = f \cdot \frac{\dot{m}^2 p_w}{8\rho A^3} \cdot L \tag{4.2}$$

where ΔP is the pressure loss due to friction, f is the friction factor, ρ is the fluid density, V is the mean flow velocity, D is the hydraulic diameter, p_w is wetted perimeter, A is area and L is the length of the segment under consideration. Coolant flowing through the pebble bed utilizes the aforementioned KTA safety standard 3102. KTA pressure drop is quantified using correlations defined by Eq. (A.10) and Eq. (A.11). Considering appropriate pressure loss correlations for each region with the functions defined in Eq. (4.1), the computed values in turn will relate all flow paths by pressure loss, characterizing the relation between the unknown mass flow rates in each gap and how they reduce the primary flow in the PBR core for each position downstream where each bypass gap is present. Applying this approach to the theoretical problem will ultimately solve for bypass gap mass flow rates based on pressure loss calculations from each function. A solution vector will be produced with evaluation of 20 unknowns, the mass flow rate for all 19 bypass gaps in the PBR domain and total pressure loss. In summary, the objective of the theoretical problem is to compute pressure loss for each possible flow path present in the PBR domain. The theoretical problem aims to provide a solution utilizing 20 functions that quantify pressure loss. Implementing this approach into a theoretical model with the premise reported will provide a solution for the first principle analysis.

Prior to discussing the approach to compute the 20 unknown values, the basis of the mathematical considerations for the theoretical problem is described. Computing pressure loss for each flow path will assume that the solutions for mass flow rates only result in positive real numbers, comparable to observations in the CFD investigation. Consequently, a constraint is defined such that the solutions for mass flow rate only have resultant values within a range of real numbers. The only defined mass flow rate is an inlet boundary condition (BC) representing the total mass flow rate in the system. By the fundamental principle, conservation of mass, bounds are placed on the system that the solutions for mass flow rate are only within the range positive real numbers defined by $[0, \dot{m}_{total}]$. Accordingly, this defines a theoretical problem constructed by

20 continuous functions. A general representation of the theoretical problem is commonly expressed as [58],

$$\begin{aligned} \min_{x} \quad & f(x) \\ \text{subject to} \quad & g_i(x) \leq 0, \quad i = 1, \cdots, m \\ & h_j(x) = 0, \quad j = 1, \cdots, p \end{aligned} \tag{4.3}$$

where $g_i(x)$ are a vector of inequality constraints, $h_j(x)$ are a vector equality constraints, and $m = p \neq 0$, in order to define the problem as constrained. The vector x that relates to the general theoretical expression consists of the design variables for the PBR model. Constraints on x are referred to as side constraints, which are modified for each case (i.e, gap size, inlet mass flow rate) for comparison to results obtained from STAR-CCM+. The additional constraints have already been mentioned above in consideration of the dataset constructed from CFD results, where it has been observed that only positive mass flow rate exist in the PBR domain, suggesting that there is no influx of bypass flow back into the reactor core. With this observation, the mass flow rates computed in the first principle analysis are expected to follow the same result and can be defined as behavioral constraints to the model. With a set of design variables defined for the PBR that fully satisfies all constraints in the theoretical problem, the solution can be computed using a non-linear multi-variable system of equations. The system of equations is constructed with the previously discussed 20 pressure loss functions with constraints. In addition, it is assumed that data for the given problem is known without inaccuracies for simplicity. This assumption defines that within the scope of the first principle analysis due to a lack of inaccuracies, the solution is obtained and neglects the possibility of any uncertainty. In result of the approach discussed, the first principle analysis is performed by developing a theoretical model with the use of appropriate software and a solver-based approach.

4.2 Model Development

With the proposed non-linear theoretical problem that conducts a first principle analysis, computing 20 unknowns is performed with appropriate numerical methods and computational

modeling. With the use of the proprietary programming language and numeric computational environment, MATLAB®, the first principle analysis can be quantified. MATLAB software is utilized since it is beneficial for general computational modeling and the necessary advanced functions to solve the non-linear theoretical problem can be implemented with a MATLAB Toolbox [59]. MATLAB code is developed with a solver-based approach and the aforementioned proposal to forming a non-linear multi-variable system of equations. Development of the theoretical model and the investigation of bypass flow employs MATLAB v. R2021a unless otherwise noted. The theoretical model developed with MATLAB employs the MathWorks optimization software package, Optimization Toolbox™. The toolbox includes a library of algorithms for non-linear programming and provides functions for finding parameters to minimize the objective functions in addition to satisfying the constraints. Applicable to the theoretical model, systems of non-linear equations are solved by finding the solution to a multi-variable, non-linear equation, $F(x) = 0$. Solvers for the system of equations transform an equation-solving problem to an theoretical approach by minimization of the sum of squares of the components of F, discussed in Section (4.1) as the theoretical problem objective. With the use of the Optimization Toolbox and MATLAB, the theoretical model for the PBR is constructed.

Developing the PBR model requires choosing an appropriate solver to solve for the unknown mass flow rates. Classification of the theoretical model in the previous section with bound constraints, a non-linear least squares solver is advantageous to acquire a feasible solution. With this determination, the non-linear least squares solver is employed with the Trust-Region-Reflective least squares algorithm. The non-linear least squares solver is a special case that resolves theoretical problems of the form,

$$\min_x \|F(x)\|_2^2 = \min_x (f_1(x)^2 + f_2(x)^2 + \cdots + f_n(x)^2) \tag{4.4}$$

$$\underset{x}{min} f^T x \text{ such that } \begin{cases} A \cdot x \leq b \\ Aeq \cdot x = beq \\ lb \leq x \leq ub \end{cases} \tag{4.5}$$

where $\underset{x}{min} f^T x$ is represented by $f^T x = f(1)x(1) + f(2)x(2) + \cdots + f(n)x(n)$ where n is the length of f. To note, minimization of the objective function with respect to the vector design variables, x, is determined as $\underset{x}{min}$. The solver allows for optional lower and upper bounds on the design variables termed as lb and ub, defined to adequately consider the aforementioned problem constraints. Linear inequality constraints are accounted for with $Ax \leq b$, representing m constraints for an n-dimensional vector x. Linear equality constraints are defined as $Aeq \cdot x = beq$ by the same form. The essential approach to solving with the non-linear least squares solver is utilizing the Trust-Region-Reflective least squares algorithm. The Trust-Region-Reflective non-linear least squares solver is computationally efficient for both small and large scale problems and is beneficial for minimization problems with constraints, such as the theoretical problem at hand [60]. For the sake of brevity, the algorithm is a beneficial Newton-step based method that determines a two-dimensional subspace to force global convergence and achieve fast local convergence while satisfying bound constraints at every iteration [61]. The utilized solver with a non-linear system of equations minimize the sum of squares of the components of F, but rather than compute the sum of squares defined in the general representation provided by Eq. (4.4), the user-defined function computes the vector-valued function by,

$$F(x) = \begin{bmatrix} f_1(x) \\ f_2(x) \\ \vdots \\ f_n(x) \end{bmatrix} \tag{4.6}$$

where each function, $f(x)$ are solved for the minimization of the the vector-valued function,

$F(x)$. For clarity, applying this to the first principles analysis becomes relatively simple, since the pressure drop for each flow path is defined using $f_n(x)$. In essence, a large contribution to defining the functions and solving the model now requires a summation of pressure drop equations that define the fluid flow path, where the pressure drop is dependent on the mass flow rate that changes at each gap downstream of the inlet. Consider the flow path through the third bypass gap downstream of the inlet, a fundamental form of the function for gap 3 (using ΔP correlations that are applicable to each region) can be quantified with mass flow rate dependence by,

$$\begin{aligned} f_3(x) = \Delta P_{cavity,1}(\dot{m}_{total} - \dot{m}_{gap,1})) \\ + \Delta P_{cavity,2}(\dot{m}_{total} - (\dot{m}_{gap,1} + m_{gap,2}) \\ + \Delta P_{gap,3}(\dot{m}_{total} - \dot{m}_{horizontal,1}) \\ + \Delta P_{vertical,4}(\dot{m}_{gap,1} + \dot{m}_{gap,2} + \dot{m}_{gap,3}) \\ + \Delta P_{vertical,5}(\dot{m}_{gap,1} + \dot{m}_{gap,2} + \dot{m}_{gap,3} + \dot{m}_{gap,4}) \\ + \Delta P_{vertical,N}(\dot{m}_N) - \Delta P_{total} = 0 \end{aligned} \tag{4.7}$$

where N is the total number of gaps, and when $N = 19$ the pressure loss calculated is at the outlet of the PBR. Note that the summation of pressure loss is subtracted by the unknown variable ΔP_{total} such that $f(x) = 0$. Consequently, this allows for the solver to obtain a solution for the total pressure drop and adjust the mass flow rates that pertain to summation of the flow path pressure loss. Within the model developed, careful consideration must be taken for mass flow rates in each pressure loss function definition. When defining the vertical gaps pressure loss, each gap segment accounts for the addition of flow from a horizontal gap, while in contrast, pressure loss through the core accounts for the loss of mass flow rate. The final step required to define the theoretical model functions is the inclusion of a mass flow rate equation that accounts for mass conservation. In summary, 19 functions are defined with a modified version of Eq. (4.7) that accounts for the

appropriate flow path, and a mass conservation function defined as,

$$\sum_{i=1}^{N-1} \dot{m}_{gaps,N} + \dot{m}_{outlet,core} - \dot{m}_{total} = 0 \tag{4.8}$$

where the summation of the bypass gap mass flow rates and the remaining mass flow in the core is required to be equivalent to the total mass flow rate defined at the inlet. In conclusion, the described approach is developed as a theoretical model that solves for bypass flow rate in all 19 gaps, in addition to a total pressure loss.

4.3 Model Procedure

Considering a PBR theoretical model analogous to CFD for comparison, the remaining process to conduct a bypass flow investigation requires consideration of geometric and thermophysical properties, which are defined in the MATLAB code accordingly. One consideration already discussed is defining the proper correlation for pressure loss, dependent of which region the flow is evaluated in. The cavity, horizontal, and vertical bypass gaps, utilize the Darcy-Weisbach pressure loss correlation shown in Eq. (4.2) and the pebble bed pressure loss is quantified with KTA safety standards defined by Eq. (A.10). Assuming the PBR is isobaric and isothermal for simplicity, the constant density value is quantified by the KTA standard for helium material properties in Eq. (A.1). A friction factor, f, must also be considered with respect to the flow regime. Assuming the flow is fully developed and the closed channels are smooth or have no roughness, the friction factor correlations for non-porous regions are characterized by the fluid flow regime present in the area of interest. Dependent on the Reynolds number to determine the applicability, friction factor is quantified as,

$$f = \begin{cases} 64/Re, & \text{for } Re < 2300 \\ (0.0790 \cdot \ln(Re) - 1.64)^{-2}, & \text{for } 3000 \leq Re \leq 5 \times 10^6 \end{cases} \tag{4.9}$$

where the laminar flow friction factor is defined by $Re < 2300$, and the Petukhov correlation used for turbulent flow requires Reynolds number in the range, $3000 \leq Re \leq 5 \times 10^6$ [62]. Petukhov friction factor is employed due to the applicability over a wide range of Reynolds numbers, however, the theoretical model takes both friction factor equations into account with a blending function that will evaluate the friction accordingly or interpolate the values using both correlations if the Reynolds number falls in the range between laminar and Petukhov friction factors. For friction factors in the bed, the correlation is expressed in KTA 3102.3 [53], where a friction loss coefficient can be quantified by Eq. (A.11). Both friction factors are dependent on Reynolds number, where the pebble bed Reynolds number is calculated using pebble diameter, representing a different length scale compared to the large cross-sectional area considered for the cavity Reynolds number.

The final considerations relate directly to the geometry of interest. For simplification of the CFD model, a two-dimensional axisymmetric domain is developed, analogous to the assumptions made in the theoretical model. This results in accounting the geometric properties of the HTR-10, and account for flow in the bypass gaps to have an area that is not constant since the gaps are rotated around a cylinder. This required the assumption of using a nominal average for the bypass gaps flow area. With these conclusions, the theoretical model developed conducts studies for varied gap size and over a range of mass flow rates ranging from 60% to 140% in an effort to compare to CFD training data to determine the feasibility of the produced results in the dataset.

5. PRONGHORN BYPASS FLOW INVESTIGATION

5.1 Computational Methodology

Pronghorn employs a computational domain of the representative PBR model comparable to STAR-CCM+ with a few variations. Pronghorn models a two-dimensional axisymmetric computational domain consisting of two blocks that are defined as the PBR pebble bed and reflector, displayed in Fig. (5.1). The pebble bed is analogous to the CFD computational domain described in Section (3.1), in addition to the HTR-10 geometric properties listed in Table (2.1). This includes modeling the active pebble bed preceding the conical zone at the bottom of the bed, where the pebbles are funneled as they approach the discharge tube. Analysis of the CFD dataset displayed each gap had no influx of helium coolant from the reflector back into the core, Consequently, flow only exits the primary flow region to the reflector. Considering this observation, for simplification, not every bypass flow gap is included in the domain. Instead of modeling 19 bypass gaps individually, a second block accounts for all gaps. The second block, referred to as the reflector, is a solid intended to be the recipient of bypass flow departing the PBR core. This simplification in Pronghorn, allows for removal of flow at each gap height without each individual gap modeled in the domain.

5.2 Governing Equations

Pronghorn has the capability to conduct multiscale analyses based on decomposing the system into several essential temporal and spatial length scales. Considering a PBR, three length scales typically describe the reactor: (1) the macroscale, which includes the reactor core in its entirety including the pebble bed, reflectors and structure; (2) the mesoscale, specified over a single pebble; and (3) the microscale, bound to a single fuel particle. The three length scales characteristic to a PBR vary over a range of six orders of magnitude, from 10^{-5} m for the smallest layer of the coated fuel particle, to 10^{1} m describing the largest dimension in the core [63]. The microscale on the order of 10^{-5} m is intended for simulating PBR applications such as temperature driven Doppler

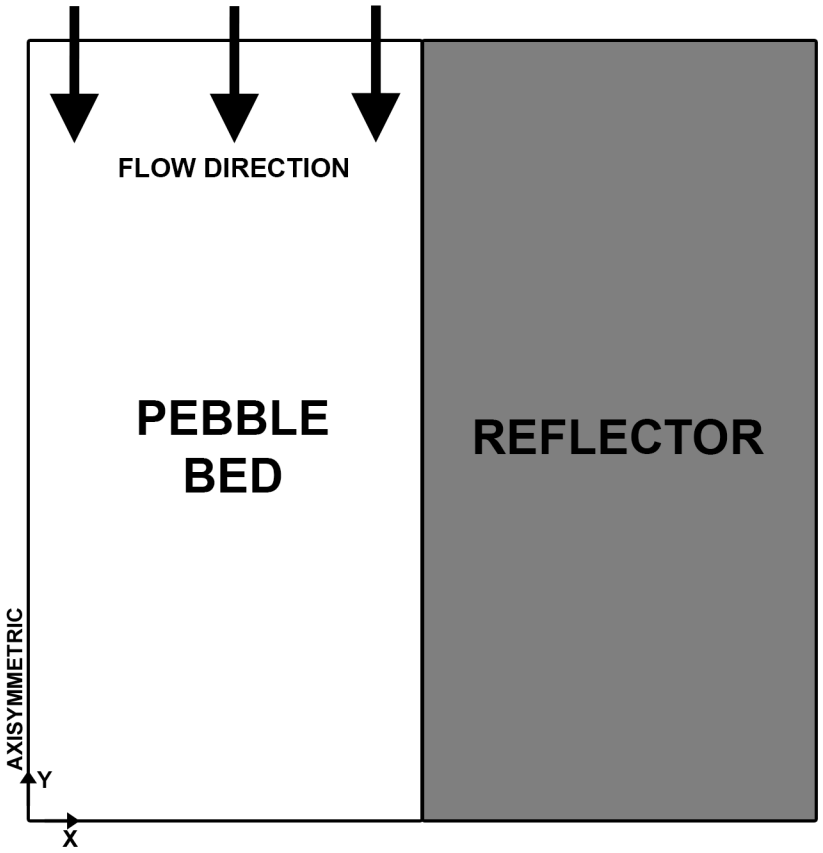

Figure 5.1: Two-dimensional axisymmetric Pronghorn model of PBR

feedback, while the macroscale of 10^1 m is relevant for heat and mass transfer effects on large-scale performance and safety criteria. For the domain of interest, a representative PBR close to the HTR-10 test reactor, a macroscale model is utilized in Pronghorn.

The macroscale model is expressed by the porous media method. The porous media method incorporates Navier-Stokes equations that govern fluid flow and heat transfer with consideration of conjugate heat transfer through the two-phase mixture of helium fluid and solid fuel pebbles. These governing equations are spatially homogenized to capture physical phenomena on the macroscale with consideration of averaged physics through model closures. This porous media modeling approach reduces computational cost while adequately capturing physical phenomena of interest.

Formulation of the porous media governing equations initially consider the conservation laws regarding compressible flow in a Newtonian continuum, as previously defined in Eqs. (3.1) -

(3.3). With the conservation laws provided, the porous media equations can then be averaged over a region, commonly referred to as the Representative Elementary Volume (REV) in macroscale models [64]. The REV contains a mixture of fluid and solid phases that result in averages insensitive to small changes in size. To conclude the porous media governing equations, a solid-fluid domain as a two-phase mixture must include porosity, ϵ, defined as the fraction of fluid to the total representative volume. Additionally, the porosity can be defined as the connected void volume to the total representative volume, as the porous medium is based on multiphase flow with interconnecting void space and consequently, the isolated voids are not considered.

$$\epsilon = \frac{\text{fluid volume}}{\text{total volume}} = \frac{\text{connected void volume}}{\text{total volume}} \tag{5.1}$$

By averaging the conservation laws over the REV with inclusion of the porosity term, formulation of the porous media governing equations are performed. The resulting governing equations include the porous media conservation of mass defined as,

$$\epsilon \frac{\partial \rho_f}{\partial t} + \nabla \cdot (\epsilon \rho_f \vec{V}) = 0 \tag{5.2}$$

where ρ_f is the intrinsic phase average of the fluid density, and $\vec{V}$ is the intrinsic phase average of the fluid velocity. In addition, the conservation of momentum is presented with the inclusion of several closure terms,

$$\epsilon \frac{\partial (\rho_f \vec{V})}{\partial t} + \nabla \cdot (\epsilon \rho_f \vec{V} \vec{V}) + \epsilon \nabla P - \epsilon \rho_f \vec{g} + W \rho_f \vec{V} - \nabla \cdot (\tilde{\mu} \nabla \vec{V}) = 0 \tag{5.3}$$

where P is the intrinsic phase average of the pressure. Finally, the conservation of energy must be defined for a thermal non-equilibrium, contrary to a majority of engineering disciplines that commonly employ thermal-equilibrium porous media modeling for investigations regarding subjects such as geophysical applications. Accounting for a thermal non-equilibrium requires inclusion of volumetric heat sources and material properties of both phases. The incorporation of

the requirements for a thermal non-equilibrium requires two unique energy conservation equations, each for the fluid and solid. Conservation of energy for the fluid phase is derived with respect to temperature by,

$$\epsilon\frac{\partial(\rho_f E_f)}{\partial t} + \nabla\cdot(\epsilon H_f \rho_f \vec{V}) - \nabla\cdot(\kappa_f \nabla T_f) - \epsilon\rho_f \vec{g}\cdot\vec{V} + \alpha(T_f - T_s) - \dot{q}_f = 0 \tag{5.4}$$

where T_f is the fluid intrinsic average temperature, $C_{p,f}$ is the intrinsic average specific heat for the fluid, H_f is the fluid enthalpy and κ_f is the intrinsic average thermal conductivity for the fluid. The convective heat transfer coefficient between the two intrinsic phase averaged temperatures is represented as α. To define the convective heat transfer coefficient with the correct units, α is represented by multiplying the heat transfer coefficient by the wetted area per unit length, a_w. The final conservation law that forms the porous media equations is attained with the same assumptions as the fluid energy conservation equation and defining $\vec{V} = 0$ since the solid does not move. Conservation of energy for the solid phase is quantified by,

$$(1-\epsilon)\rho_s C_{p,s}\frac{\partial T_s}{\partial t} - \nabla\cdot(\kappa_s \nabla T_s) + \alpha(T_s - T_f) - \dot{q}_s = 0 \tag{5.5}$$

where κ_s is the effective solid thermal conductivity, ρ_s is the intrinsic average of the solid density, $C_{p,s}$ is the intrinsic average of the solid specific heat and $\dot{q}_s$ is the extrinsic average of the solid volumetric heat source. The set of porous media governing equations is commonly referred to as the Navier-Stokes model [65]. Pronghorn also includes a Euler model and friction-dominated model which all are compressible flow models with identical solid energy conservation equations.

5.2.1 Friction-Dominated Model

With the Navier-Stokes porous media governing equations presented for macroscale models, a few changes must be made to have an applicable model for the representative PBR based on the HTR-10. Since the HTR-10 is a test reactor and has a significantly lower reactor coolant flow rate, a model must consider slowly-evolving, low Reynolds number flow [66]. In this case, the

friction-dominated model is applied assuming that the momentum conservation is dominated by the friction effects, resulting in change of pressure instantaneously reflected as changes in momentum. Incorporating a friction-dominated under these assumptions is possible by defining the total derivative of momentum displayed in Eq. (5.3) to zero, resulting in a pseudo-steady momentum equation.

$$\epsilon \nabla P - \epsilon \rho_f \vec{g} + W \rho_f \vec{V} = 0 \tag{5.6}$$

The pseudo-steady momentum equation is then substituted into a conservation of thermal energy considering specific volume and temperature to produce the pressure Poisson equation,

$$\epsilon \frac{\partial \rho_f}{\partial t} + \nabla \cdot \left[\frac{\epsilon^2}{W} (\rho_f \vec{g} - \nabla P) \right] = 0 \tag{5.7}$$

To conclude defining the friction-dominated model, the conservation of internal energy is typically used due to compression work primarily being negligible for slowly-evolving flows. Conservation of internal energy is stated as,

$$\epsilon \rho_f C_{p,f} \frac{\partial T_f}{\partial t} + \epsilon \rho_f C_{p,f} \vec{V} \cdot \nabla T_f + \nabla \cdot (\kappa_f \nabla T_f) + \alpha (T_f - T_s) - \dot{q}_f = 0 \tag{5.8}$$

In summary, from the three available macroscale models available in Pronghorn (Navier-Stokes, Euler, Friction-dominated), the friction-dominated model is the most applicable with respect to the flow present in the HTR-10. The porous media governing equations for the friction-dominated model are presented in Eqs. (5.6-5.8). The strong form of the friction-dominated model equations is defined, which typically consist of the governing equations as Partial Differential Equations (PDEs) and boundary conditions for a system. To solve for the governing equations in Pronghorn, the Finite Element Method (FEM) is employed, which is notably different from the FVM commonly used in CFD and incorporated in STAR-CCM+. With the strong form governing equations discussed, solving the PDE using FEM needs to take into consideration the weak Galerkin finite element form, where the strong form equations are expressed in an integral form of

the governing PDEs termed the weak form, which are necessary to formulate the FEM [67]. The weak form of the governing PDEs for the friction-dominated model in Pronghorn are defined in the set of equations below.

$$\int_{\Omega} \epsilon \frac{\partial \rho_f}{\partial t} \Psi d\Omega - \int_{\omega} \left[\frac{\epsilon^2}{W} (\rho_f \vec{g} - \nabla P) \right] \cdot \nabla \Psi d\Omega + \int_{\Gamma}) \left[\frac{\epsilon^2}{W} (\rho_f \vec{g} - \nabla P) \right] \Psi d\Gamma = 0, \tag{5.9a}$$

$$\int_{\Omega} \left[-\epsilon \rho_f g_i + W \rho_f V_i - P \frac{\partial \epsilon}{\partial x_i} \right] \Psi d\Omega - \int_{\Omega} \epsilon P \frac{\partial \Psi}{\partial x_i} d\Omega + \int_{\Gamma} \epsilon P n_i \Psi d\Gamma = 0, \tag{5.9b}$$

$$\begin{aligned} \int_{\Omega} \left[\epsilon \rho_f C_{p,f} \frac{\partial T_f}{\partial t} + \epsilon \rho_f C_{p,f} \vec{V} \cdot \nabla T_f + \alpha (T_f - T_s) - \dot{q}_f \right] \Psi d\Omega \\ + \int_{\Omega} [\kappa_f \nabla T_f \cdot \nabla \Psi d\Omega] - \int_{\Gamma} \kappa_f \nabla T_f \cdot \hat{n} \Psi d\Gamma = 0, \end{aligned} \tag{5.9c}$$

$$\begin{aligned} \int_{\Omega} \left[(1-\epsilon) \rho_s C_{p,s} \frac{\partial T_s}{\partial t} + \alpha (T_s - T_f) - \dot{q}_s \right] \Psi d\Omega + \\ \int_{\Omega} \kappa_s \nabla T_s \cdot \nabla \Psi d\Omega - \int_{\Gamma} [\kappa_s \nabla T_s \cdot \hat{n} \Psi d\Gamma] = 0 \end{aligned} \tag{5.9d}$$

5.3 Computational Procedure

Pronghorn performs all cases of varying mass flow rate and gap size using the two block computational domain consisting of a pebble bed and a solid reflector with the friction-dominated macroscale model discussed in Section (5.2.1). Pronghorn requires the friction-dominated model to be defined with a set of variables, which has the option to incorporate conserved variables, primitive variables and mixed variables. Pronghorn for all cases in this study employs a mixed variable set that solves the fluid model with superficial momentum, pressure and temperature. One benefit to using superficial momentum is the resulting improved convergence for problems with significant porosity spatial gradients. As for stabilization, the friction-dominated model

stabilizes the mass and energy equation against each other in consideration of the lack of an advective term.

Viscous and inertial drag scales are available in all Pronghorn models, and can be represented in as the interphase friction factor, W, for pebble bed correlations assuming randomly-packed beds of smooth, uniform diameter spheres. Pebble bed correlations define coefficients A and B that can be applied to the friction drag scale formulas representative of pressure drop,

$$-\nabla P \frac{\epsilon^3}{1-\epsilon} \frac{d_p}{\rho v^2} = A \frac{1-\epsilon}{Re} + B, \tag{5.10a}$$

$$-\nabla P \frac{\epsilon^3}{(1-\epsilon)^2} \frac{d_p^2}{\mu v} = A + B \frac{Re}{1-\epsilon} \tag{5.10b}$$

where Eq. (5.10a) is normalized by the dynamic pressure and Eq. (5.10b) is normalized by the viscous shear stress. Analogous to the CFD model, the pebble bed friction factor is quantified considering the inertial and viscous drag with the KTA drag model defined in Eq. (A.13). Two lengths are presented in the KTA drag model regarding the hydaulic and pebble bed diameters D and d_p, and two velocity scales are present in the Reynolds number definitions. Hydraulic diameter can be defined when the fluid flow volume is represented by $\forall_f = \epsilon \forall$, with an absence of wall effects in the bulk of a bed of spherical pebbles by,

$$D = \frac{4\epsilon}{6(1-\epsilon)} d_p \tag{5.11}$$

where commonly the factor of 4/6 in the calculation is ignored. The two characteristic length scales can be quantified for determining the Reynolds number, depending on whether the velocity scale considers the interstitial velocity, V, or superficial velocity, v. The interstitial velocity is commonly referred to as the physical velocity and represents the theoretical development of the physical flow as it enters a porous medium. When flow enters the porous medium, the velocity rises due to the decrease in flow area. Superficial velocity is common in porous media modeling and is an artificial velocity that is homogenized in the fluid and solid neglecting the increase in

physical velocity. These two velocity scales are related by,

$$v = \epsilon \cdot V \tag{5.12}$$

where ϵ is the porosity of the pebble bed. With the two length scales and velocity scales considered, the Reynolds number can be defined as,

$$Re = \frac{\rho v d_p}{\mu}, \tag{5.13a}$$

$$Re_h = \frac{\rho V D}{\mu} \tag{5.13b}$$

where Re in Eq. (5.13a) is the Reynolds number concerning pebble diameter and superficial velocity, while Re_h in Eq. (5.13b) is the hydraulic Reynolds number regarding interstitial velocity and hydraulic diameter in the bulk of the bed. Both Reynolds numbers must be considered when determining if the KTA drag model is applicable to the PBR model at hand, in addition to quantifying the friction in the pebble bed if the KTA drag model is implemented.

6. RESULTS

To summarize the outcome of the various PBR models considered and presented subsequently, results for the bypass flow in the PBR and other related parameters of interest are computed using the methodology and procedures discussed in the preceding sections for this investigation. CFD modeling using FVM is described in detail in Chapter (3), a first principle analysis is performed as expressed in Chapter (4), and the MOOSE-based application, Pronghorn, conducts the appropriate simulations designated in Chapter (5). All cases for varying total mass flow rate and gap sizes are satisfied with each computational tool, respectively.

6.1 CFD Results

Results for the representative PBR model include cases for multiple gap sizes ($\delta = 1, 2, 3$ mm) and total mass flow rates. Total mass flow rates are defined as the PBR inlet BC ranging in increments of 20% within 60% to 140% of the HTR-10 core mass flow rate under normal operating conditions that effectively cool the core (i.e., $\dot{m}_{total} = 3.7584\ kg/s$ for the 100% case). Results for the three gap size cases are listed in Table (6.1), where the significant parameters of interest are the mass flow fractions for primary and bypass flow. The mass flow fraction is determined by the total mass flow rate at the outlet per total mass flow rate at the inlet either for the entire primary flow or bypass flow region.

Table 6.1: CFD bypass flow results for a PBR under 100% normal operating conditions for gap sizes $\delta = 1, 2, 3$ mm

	Normal Operation at 100%		
δ (mm)	ΔP (Pa)	Primary (%)	Bypass (%)
1.00	482.416	99.0719	0.92808
2.00	447.355	93.7045	6.29552
3.00	395.562	85.4423	14.5577

For each gap size, the total pressure loss and mass flow fractions on first glance do not show any distinguishable results that are contrary to expectations. As the gap size is increased, the amount of flow that departs the primary flow region follows suit. In comparison to primary flow, larger gap sizes have an adverse effect on the amount of bypass flow present in the PBR, increasing significantly when gap size is uniformly expanded by a single millimeter. PIRT studies discussed in Section (2.3) have demonstrated concern for bypass flow phenomena, not only due to resulting excess bypass flow, but also on account of the challenges faced when estimating bypass flow for numerous reasons. This holds true when attempting to compare bypass flow results to the HTR-10, as steady-state and transient analyses have been published [68, 69], but to this author's knowledge, a lack of concrete data is available under various operating conditions. At most, previous literature has stated that total bypass flow present in the HTR-10 has been reported as having potential to be reduced to be less than 10% of the total flow with the presence of keys and dowels connecting the graphite blocks, but should not exceed 14% [70, 71]. Cases with the assorted gap sizes represent this conclusion, as the representative PBR with uniform 3 mm gaps resulting in a bypass flow fraction that is roughly 14%. Considering the representative PBR domain that is employed for the CFD studies, there are 19 gaps modeled out of the 20 present in the HTR-10 design, both circumferentially and vertically. The loss of flow in the primary region occurs incrementally, as each bypass gap gains an amount of the fluid that was previously present in the core. The mass flow rate that is present in both the PBR core and bypass gap is displayed in Fig. (6.1), where the average mass flow rate is reported at a position downstream of the cavity inlet equivalent to each of the bypass gaps present in the PBR model. By observation, the primary region loses a significant amount of coolant in the cavity of the PBR, an expected occurence in the HTR-10 that serves as merit to maintain various components functions outside the core. Since the helium coolant enters the upper plenum from cold helium risers at a temperature of 250 °C and subsequently advances through the cavity, fluid entering the bypass gaps from the cavity is significantly lower in temperature than the pebble bed, which supports some of the structures in the side reflector such as control rod cladding.

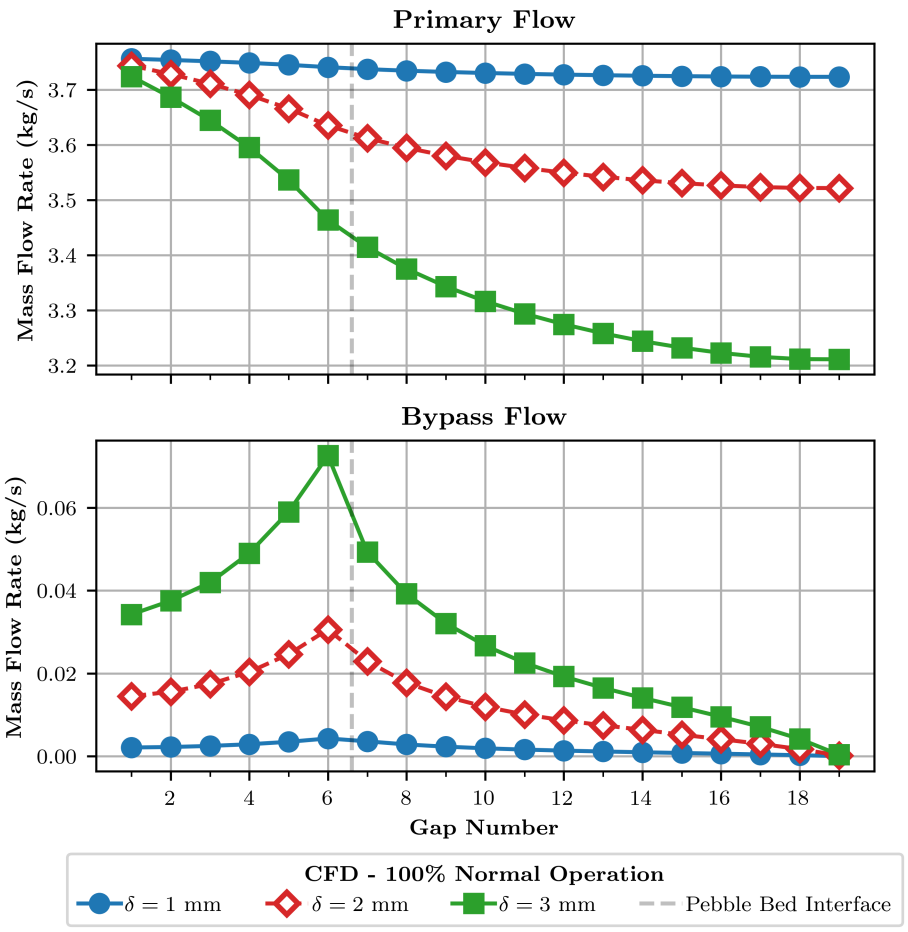

Figure 6.1: Primary and bypass average mass flow rate at each gap downstream from the PBR inlet for gap sizes $\delta = 1, 2, 3$ mm

Introducing the pebble bed to the fluid flow significantly reduces the mass flow rate due to the presence of the fuel pebbles that now occupy a portion of the flow path. The once open area that helium traveled through now is crowded with thousands of fuel pebbles that appreciably reduce the flow area and divide it into numerous interstitial paths for the coolant to travel. Consequently, flow through the pebble bed results in a signficant pressure drop, in comparison to the near-constant pressure in the cavity, as presented in Fig. (6.2) for all gap sizes. It can be seen the pebble bed is where a majority of the pressure loss occurs in the PBR core, and in correspondence with the pressure in the side reflectors, a large pressure differential results. Difference in pressure between the core and the side reflector assists as a driving force behind creating the bypass flow in the PBR.

For the flow to travel through the bypass gaps, a pressure differential must exist to drive the fluid from the core to side reflector. In a PBR, it is clear that avoiding all bypass flow is not feasible for multiple reasons. First, since gaps between the graphite blocks are separated to account for thermal expansion, the presence of bypass gaps and possible flow paths for the coolant can't be eliminated. Second, the large pressure loss produced by the pebble bed will cause a pressure gradient between the core and side reflector, inevitably generating the driving force to propel the coolant through the bypass gaps.

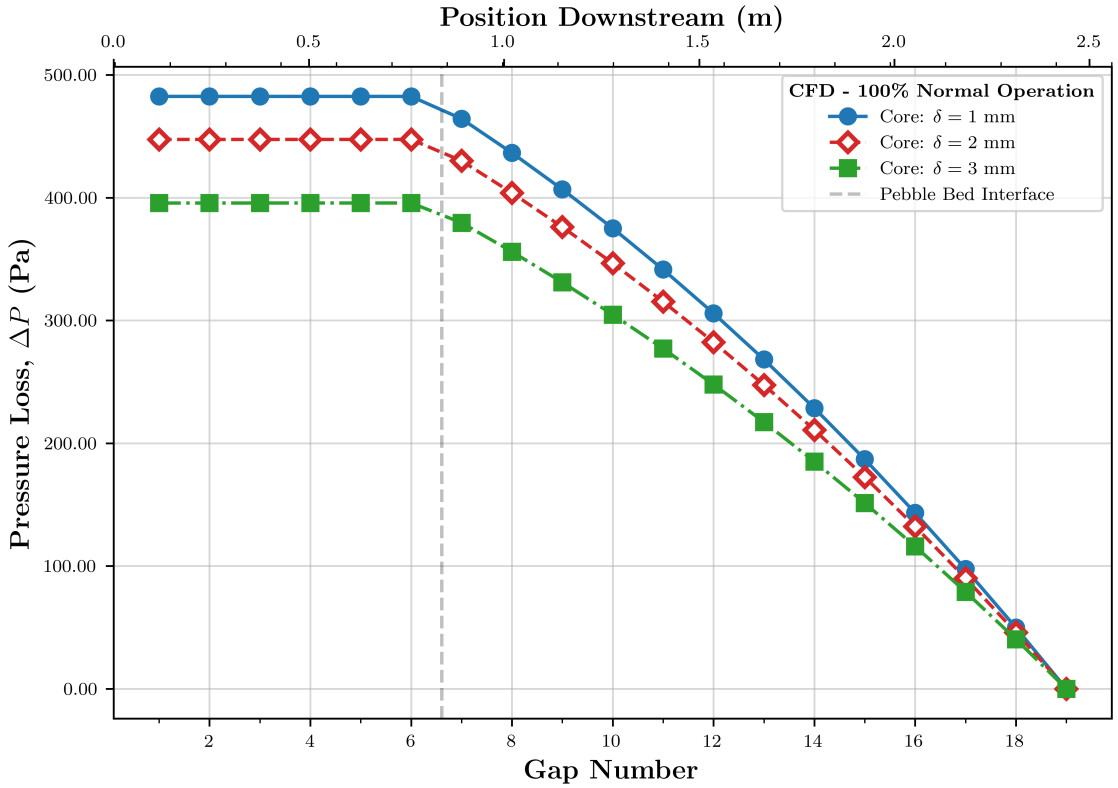

Figure 6.2: Average pressure in the PBR core at each gap position downstream with 100% normal operating conditions for gap sizes $\delta = 1, 2, 3$ mm

To summarize, the presented results for the PBR model obtained using STAR-CCM+, display characteristics that are representative of a PBR and the HTR-10. As previously stated, a primary concern resulting from excess bypass flow in a PBR, is the lack of efficiently cooling the pebble bed

due to excess bypass flow, raising T/H safety concerns from the insufficient heating. To observe the impact of bypass flow to the reactor temperature, a centerline of temperature in the PBR core is displayed in Fig. (6.3), confirming the expected temperature rise regardless of gap size. With the gap size of 3 mm gaps, under 100% normal operation, the resultant bypass flow fraction rate is slightly above 14%, which is the maximum percent of bypass flow the HTR-10 should experience. Since the 3 mm bypass gaps accrue the most bypass flow in comparison to other cases of the present study, the centerline temperature matches expectations that 3 mm gaps endure the highest temperatures due to primary flow loss. For varied mass flow rate cases ranging from 60% to 140%, results are tabulated for Figures (B.3) - (B.5) in Appendix B.

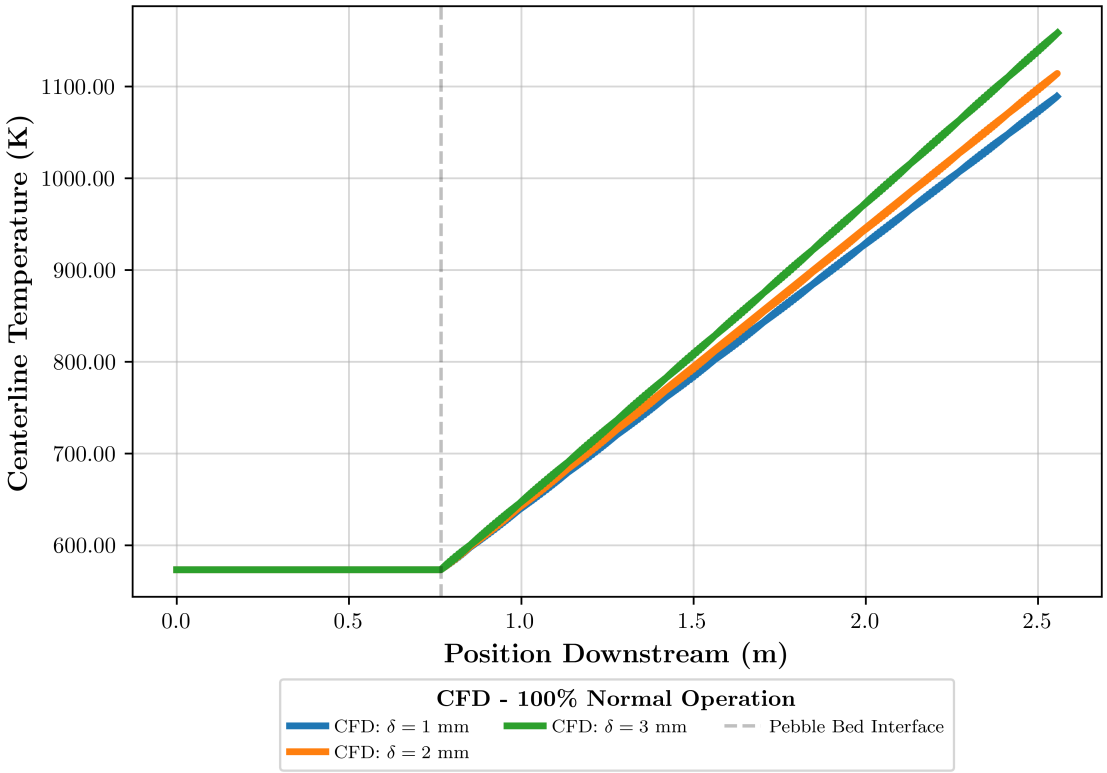

Figure 6.3: Axial centerline temperature in the PBR core considering gaps $\delta = 1, 2, 3$ mm at 100% normal operating conditions.

In result, the majority of interstitial gaps are considered in the bypass region, which can be

indicative of the bypass flow detailed in this study regarding the HTR-10 design. It is notable, however, that assumptions for the PBR model neglecting the conus, lower plenum, and core components could alter the presence of bypass flow in the reactor. Nevertheless, CFD studies conducted with uniform distribution of gap size from 1 to 3 mm exhibit the bypass flow dependence on the size of the interstitial flow paths has significant influence on the amount of helium coolant that is removed from the core. This conclusion reiterates concerns in consideration of PBR designs, especially with respect to the graphite blocks. Although it is assumed graphite blocks disregard any thermal- or irradiation-induced deformation, over the period of PBR operation this occurrence will affect the graphite blocks geometry and alter the gap size, thus resulting in possible increased bypass flow.

Concluding that size of the gap plays a major role on the presence of bypass flow present in the PBR, further investigation needs to be conducted to identify if other parameters contribute as a major or minor factor to bypass flow. For this reason, the total mass flow rate that is defined at the inlet is analyzed over a range of 60% to 140% of the total mass flow rate in the HTR-10 under normal operating conditions. The range for mass flow rates is defined in increments of 20%, providing 5 total mass flow rates (60%, 80%, 100%, 120%, 140%) of concern. Mass flow rate is considered as a parameter to investigate due to the applicability that it may be adjusted in numerous situations. In the event that small power fluctuations occur, scaling back or increasing the mass flow rate may be a necessary action in reactor operation, and although it may be a feasible task to adjust for, the mass flow rate could create the possibility of either a greater bypass flow fraction in the reactor or a lower fraction. Depending on the severity of the increase or decrease of bypass flow, the change in mass flow rate could lead to further implications. All 5 mass flow rates were conducted with gap sizes of 1, 2, and 3 mm and tabulated in Table (6.2) to investigate the affect mass flow rate has on the resulting bypass flow. With this determination, it can be evaluated whether situations that require adjustment of the mass flow rate in the reactor may have a significant impact on the presence of bypass flow or not.

Table 6.2: CFD results for gap sizes $\delta = 1, 2, 3$ mm considering total mass flow rates ranging between 60% to 140%.

		$\delta = \mathbf{1\ mm}$		
Range (%)	$\dot{m}_{total}$ (kg/s)	ΔP (Pa)	Primary (%)	Bypass (%)
60.00	2.25504	230.950	99.2352	0.76484
80.00	3.00672	346.329	99.1608	0.83923
100.0	3.75840	482.418	99.0719	0.92808
120.0	4.51008	638.685	98.9727	1.02729
140.0	5.26176	814.930	98.8802	1.11975
		$\delta = \mathbf{2\ mm}$		
Range (%)	$\dot{m}_{total}$ (kg/s)	ΔP (Pa)	Primary (%)	Bypass (%)
60.00	2.25504	218.205	94.7037	5.29631
80.00	3.00672	323.767	94.1557	5.84430
100.0	3.75840	447.355	93.7045	6.29552
120.0	4.51008	588.686	93.3540	6.64599
140.0	5.26176	747.965	93.1152	6.88480
		$\delta = \mathbf{3\ mm}$		
Range (%)	$\dot{m}_{total}$ (kg/s)	ΔP (Pa)	Primary (%)	Bypass (%)
60.00	2.25504	194.711	86.2402	13.7598
80.00	3.00672	287.117	85.7439	14.2561
100.0	3.75840	395.562	85.4423	14.5577
120.0	4.51008	519.275	85.1941	14.8059
140.0	5.26176	658.104	84.9839	15.0106

From the data presented in Table (6.2) above, the respective range of mass flow rates chosen appear to have little or no effect on bypass flow in the PBR. It appears at first glance that the largest change to the PBR is pressure loss which is expected since it holds true to the mass flow rate dependence for a smaller or larger result. With increasing mass flow rates, the amount of bypass flow increases, however, the percent of bypass flow present does not rise significantly. In reference to 3 mm gaps, the primary mass flow rate at each gap downstream of the inlet is shown in Fig. (6.4), where the mass flow present in the PBR for each case follow the same trend regarding amount of flow leaving the primary flow region as the coolant traverses through the PBR.

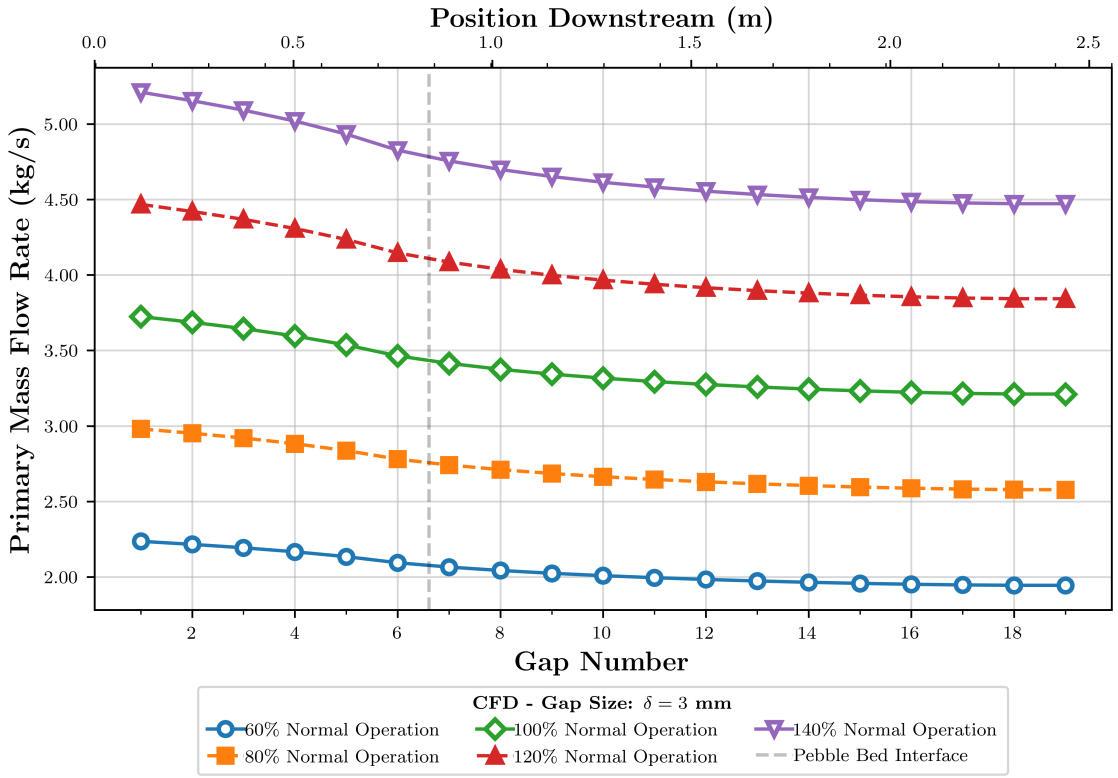

Figure 6.4: Primary mass flow rate in the core for 3 mm gap cases with varied mass flow rates

Although the mass flow rates in the PBR are decreased or increased by up to 40%, the behavior of primary flow in the core follows the same trend in each case. Unlike the observation when the size of the gaps between graphite blocks is modified, it seems that the total mass flow rate

distribution in the PBR has very small differences. In each instance, the resulting pressure loss is the only parameter that experiences a notable decrease or increase in result. For the bypass flow, the mass flow rate acquired from the primary region at each gap downstream from the PBR inlet is presented in Fig. (6.5) below.

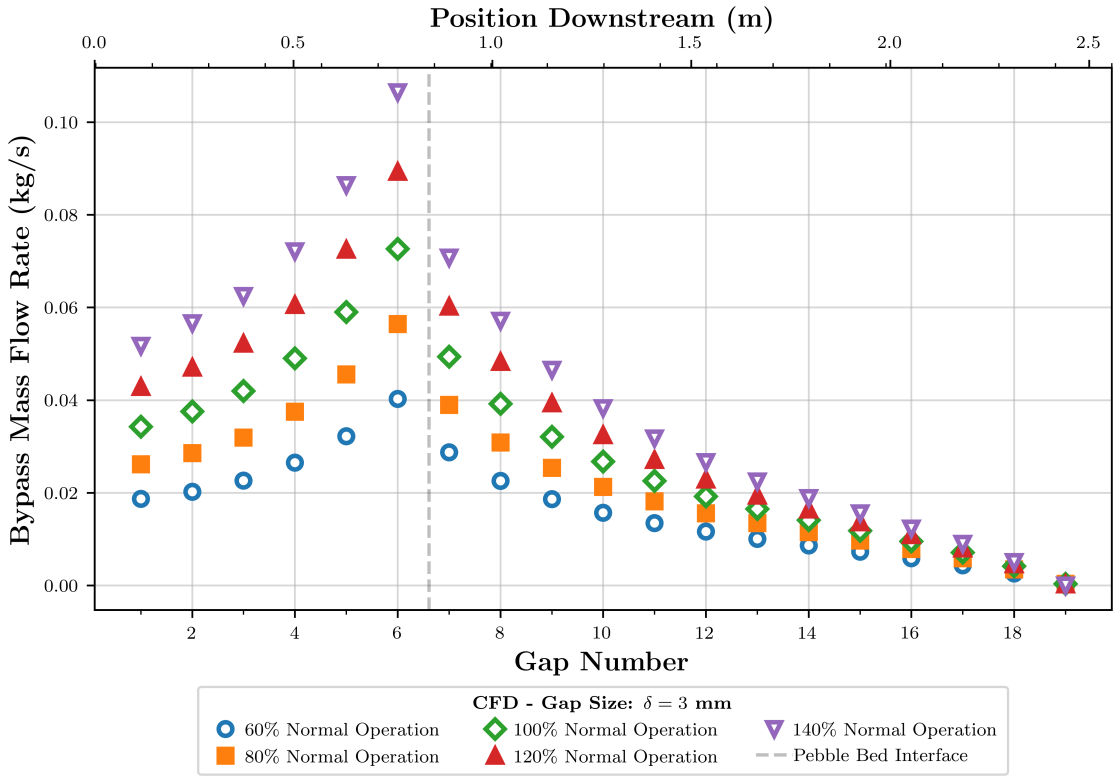

Figure 6.5: Primary mass flow rate in the core for 3 mm gaps with varied mass flow rates.

Since the range of mass flow rates considerably vary in value, the scale for the primary flow rates shown qualitatively make it difficult to see any change of flow in the PBR, however, bypass flow rates for each gap leave the primary region for all mass flow rate cases. From the figure shown above, each total mass flow rate result follows a similiar trend, especially in the cavity where it is observed that a significant amount of the total bypass flow is acquired. As flow is traveling through the second half of the bed near the outlet, considerably less flow leaves the primary region in each instance. Near the outlet of the reactor and the final gaps modeled in the representative PBR, the

amount of flow present in the bypass gaps are significantly lower values in comparison to gaps in the cavity and upper pebble bed. This can be atttributed to the pressure loss decreasing down the position of the bed. As previously discussed, bypass flow is driven by the pressure gradient between the core and the side reflector, and referencing back to Fig. (6.2), the pressure loss in the core for the final 2 gaps is roughly 10% of the total pressure loss in the PBR, resulting a smaller pressure gradient and less flow directed into the side reflector. With respect to the CFD model considered, the results are typical of what is expected in a PBR, however, consideration of the lower portion of the PBR such as the conus would lead to a higher pressure drop value and results of a domain with the conus may not match the presented results. This however does not disprove the significance of total mass flow rate, but follows the same tendencies. By analyzing the variation in bypass flow present in the PBR, the total mass flow rate does not pertain to significant changes in loss of flow in the core. Regardless of the gap size, the resulting variation in bypass flow displays the minor role contributed to total bypass flow in the PBR. For reference regarding primary mass flow rate and bypass flow rate by position downstream in the PBR, the figures are tabulated in Appendix B and shown in Fig. (B.1) and Fig. (B.2), accordingly.

6.2 First Principle Analysis Results

In short, results from Section (6.1) demonstrate the representative PBR model bypass flow is primarily dependent on the size of the gap that separates one graphite block from another in the side reflector. Results for primary and bypass flow are similar to what is expected theoretically in a typical PBR. The first principle analysis conducted investigates cases for multiple gap sizes ($\delta = 1, 2, 3$ mm) and total mass flow rates analogous to the studies performed using the the finite volume commercial CFD software. The first principle analysis efforts are made in an effort to compare the results from the CFD investigations. To initially compare primary flow and bypass flow computed in both investigations, results for all gap sizes are tabulated in Table (6.3).

In reference to the computed mass flow fractions, both the CFD model and theoretical model agree well. Bypass flow fractions computed for gaps, $\delta = 1, 2, 3\ mm$, have relatively reasonable results that correspond to each other. It is noteworthy to address the pressure loss values produced

Table 6.3: Comparison of CFD and theoretical model results for various gap sizes.

	CFD Model			**Theoretical Model**		
δ (mm)	ΔP (Pa)	Primary Flow (%)	Bypass Flow (%)	ΔP (Pa)	Primary Flow (%)	Bypass Flow (%)
1.00	482.416	99.0719	0.92808	350.755	99.4232	0.57683
2.00	447.355	93.70448	6.29552	329.077	95.7011	4.29887
3.00	395.562	85.4423	14.5577	269.435	84.8738	15.1262

using both resources differ by a considerable amount, however, both models appear to agree with pressure loss values appropriate with the assumptions given to each model, respectively. To elaborate, pressure loss is quantified appropriately in a simple manner with consideration of the cavity and the pebble bed below to demonstrate the feasibility of the results generated by the non-linear least squares theoretical model.

Assuming the PBR model is absent of all bypass gaps, loss is calculated in the cavity with Eq. (4.2) and pebble bed using Eq. (A.10).

$$\Delta P = \Delta P_{cavity} + \Delta P_{bed} = 353.884\ Pa \tag{6.1}$$

The pressure loss for the simplified example in Eq. (6.1) is comparable to the 1 mm gaps case quantified by the theoretical model, thus demonstrating the feasibility of the pressure loss results. Since the theoretical model does not consider heat generation, the pressure loss results in all cases will be underreported in comparison to those obtained using CFD. With the constraints utilized in the theoretical model to consider mass conservation, however, the mass flow rates obtained can closely represent CFD results for further comparison.

Considering all cases regarding gap size for the CFD and theoretical models, primary flow rate and bypass flow rate can be seen in Fig. (6.6) at the position of each bypass gap downstream of the PBR inlet. In the figure, the size of the gap is referred to by the markers. For both models, primary and bypass flow values correlate with small differences. In addition, the greatest amount of mass

flow gained in the bypass flow region is at the sixth gap, just prior to the entrance of the pebble bed. The trend of flow lost from the primary region per position downstream in the theoretical model concurs with CFD data.

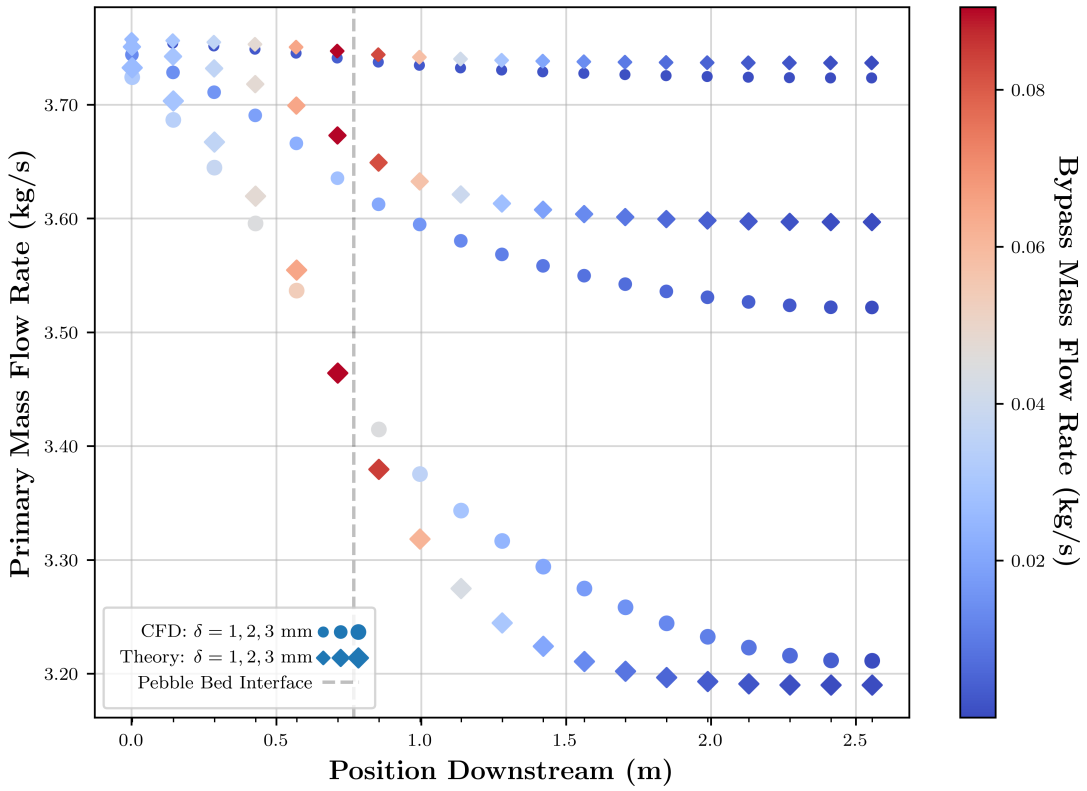

Figure 6.6: Core and bypass mass flow rate at each gap for all gap size cases ($\delta = 1, 2, 3$ mm)

By observation, the overall conclusion considering the gap size studies is that the theoretical model results for mass flow rates are in favor of the CFD data. The underprediction and overpredicted values from the theoretical model can be attributed to the assumptions made. Primary flow rates for 1 mm and 2 mm gaps are underreported utilizing the theoretical model compared to CFD data, which could be a consequence from underpredicting the total pressure loss for the PBR. With isothermal assumptions, even considerations of material properties such as helium will result in pressure loss results that are lower than expected. On the other hand, the

overestimated mass flow rates for the 3 mm gap case can pertain to the simplified approach of using friction factors without consideration of loss coefficients such as entrance/exit affects amongst other parameters that could be considered in the theoretical model. For a greater insight, the bypass flow rates computed, refer to Fig. (6.7). Total mass flow rates ranging from 60% to 140% under normal operating conditions were also computed and listed in Table (6.4) for comparison.

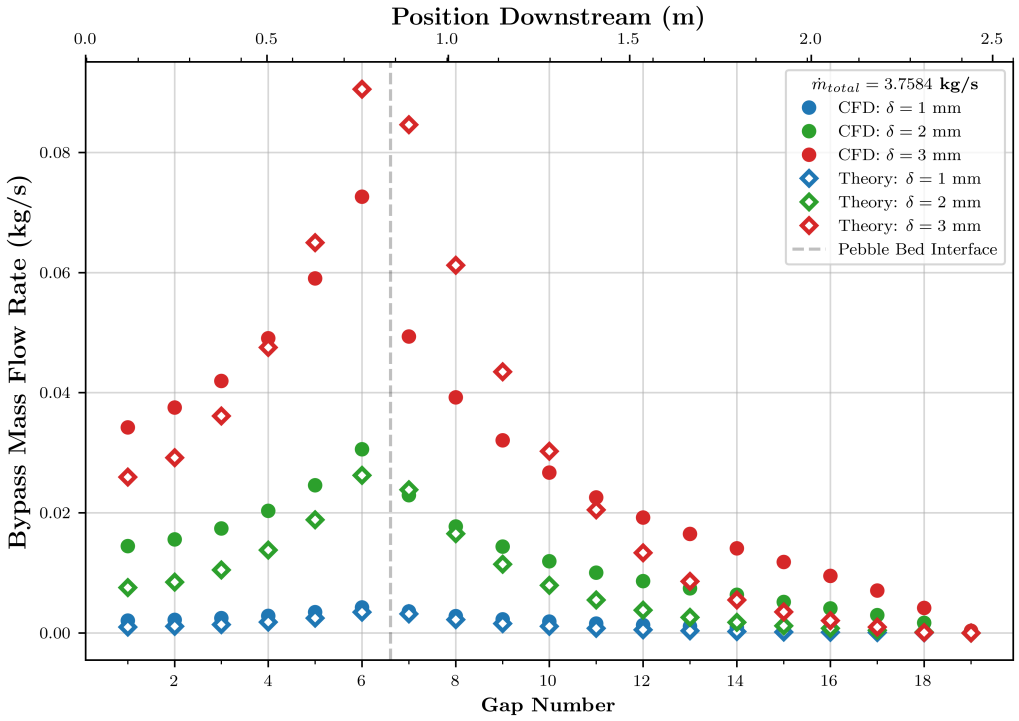

Figure 6.7: Core and Bypass Mass Flow Rate at Each Gap for all gap size cases ($\delta = 1, 2, 3$ mm)

Table 6.4: CFD and theoretical model results for gap sizes $\delta = 1, 2, 3$ mm considering total mass flow rates ranging between 60% to 140%.

$\delta = \mathbf{1\ mm}$		**CFD Model**			**Theoretical Model**		
Range (%)	$\dot{m}_{total}$ (kg/s)	ΔP (Pa)	Primary (%)	Bypass Flow (%)	ΔP (Pa)	Primary (%)	Bypass (%)
60.00	2.25504	230.950	99.2352	0.76484	135.385	99.6288	0.37121
80.00	3.00672	346.329	99.1608	0.83923	231.277	99.5245	0.47552
100.0	3.75840	482.418	99.0719	0.92808	350.755	99.4232	0.57683
120.0	4.51008	638.685	98.9727	1.02729	493.164	99.3243	0.67575
140.0	5.26176	814.930	98.8802	1.11975	657.987	99.2273	0.77267
$\delta = \mathbf{2\ mm}$		**CFD Model**			**Theoretical Model**		
Range (%)	$\dot{m}_{total}$ (kg/s)	ΔP (Pa)	Primary (%)	Bypass Flow (%)	ΔP (Pa)	Primary (%)	Bypass (%)
60.00	2.25504	218.205	94.7037	5.29631	129.903	97.1645	2.83554
80.00	3.00672	323.767	94.1557	5.84430	219.377	96.4135	3.58673
100.0	3.75840	447.355	93.7045	6.29552	329.077	95.7011	4.29887
120.0	4.51008	588.686	93.3540	6.64599	457.847	95.0217	4.97830
140.0	5.26176	747.965	93.1152	6.88480	598.920	93.6013	6.39874
$\delta = \mathbf{3\ mm}$		**CFD Model**			**Theoretical Model**		
Range (%)	$\dot{m}_{total}$ (kg/s)	ΔP (Pa)	Primary (%)	Bypass Flow (%)	ΔP (Pa)	Primary (%)	Bypass (%)
60.00	2.25504	194.711	86.2402	13.7598	117.365	91.4436	8.55643
80.00	3.00672	287.117	85.7439	14.2561	188.674	87.7041	12.2959
100.0	3.75840	395.562	85.4423	14.5577	269.435	84.8738	15.1262
120.0	4.51008	519.275	85.1941	14.8059	374.633	84.6638	15.3362
140.0	5.26176	658.104	84.9839	15.0106	497.195	84.5012	15.4988

6.3 Pronghorn Results

To conclude this bypass flow investigation, the MOOSE-based application, Pronghorn, is utilized to exhibit capabilities of accounting for a presence of bypass flow in a PBR. Data accumulated for gaps $\delta = 1, 2, 3$ mm, as well as cases regarding total mass flow rate varying from 60% to 140%, are utilized in Pronghorn. The output quantities obtained from the CFD dataset were implemented as input values in Pronghorn utilizing the PiecewiseConstant function as a Dirichlet BC on the pebble bed and reflector interface. With the described process, this study aims to prove the feasibility of Pronghorn quantifying primary and bypass mass flow rates.

Analogous to CFD and theoretical model studies, Pronghorn models are considered for multiple gap sizes, $\delta = 1, 2, 3\ mm$, and all mass flow rate cases. Since the Pronghorn model described in Section (5.1) only consists of the pebble bed and disregards the cavity, the inlet mass flow rate for each case is obtained by acquiring the cavity and pebble bed interface mass flow rate in STAR-CCM+. The mass flow rates were then quantified as mass flux values for Pronghorn input. For all 3 gap sizes, Pronghorn utilized the amount of primary flow to remove at each gap by a Dirichlet BC, tabulating the results for comparison with CFD in Table (6.5).

Table 6.5: Comparison of CFD and theoretical model results for various gap sizes.

	Pronghorn Model			**CFD Model**		
δ (mm)	ΔP (Pa)	Primary Flow (%)	Bypass Flow (%)	ΔP (Pa)	Primary Flow (%)	Bypass Flow (%)
1.00	484.529	97.0812	2.91880	482.416	99.0719	0.92805
2.00	432.394	94.0464	5.95360	447.355	93.7045	6.29552
3.00	411.981	87.0716	12.9284	395.562	85.4422	14.5578

The results reported in the table above appear at first glance that Pronghorn corresponds with the CFD simulations adequately. To illustrate the results for further comparison, the average mass flow rate in the core at each 3 mm gap location downstream of the PBR inlet for Pronghorn,

CFD, and the theoretical model is displayed in Fig. (6.8). Evaluating the results for primary and bypass flow in the pebble bed, Pronghorn compares relatively well to the other models employed, however, the consideration that the flow is explicitly removed by a function and Dirichlet BC with identical values obtained from STAR-CCM+, the expectation is that the mass flow rates between CFD results and Pronghorn should be nearly identical. The table above shows the same trend as the 3 mm plot, Pronghorn agrees with the data generated from CFD and the theoretical model, but continues to have a relative difference of about 2% for each case. For reference to the 1 mm and 2 mm gaps results, the primary mass flow rate downstream of the bed inlet is displayed in Figures (B.9) and (B.10).

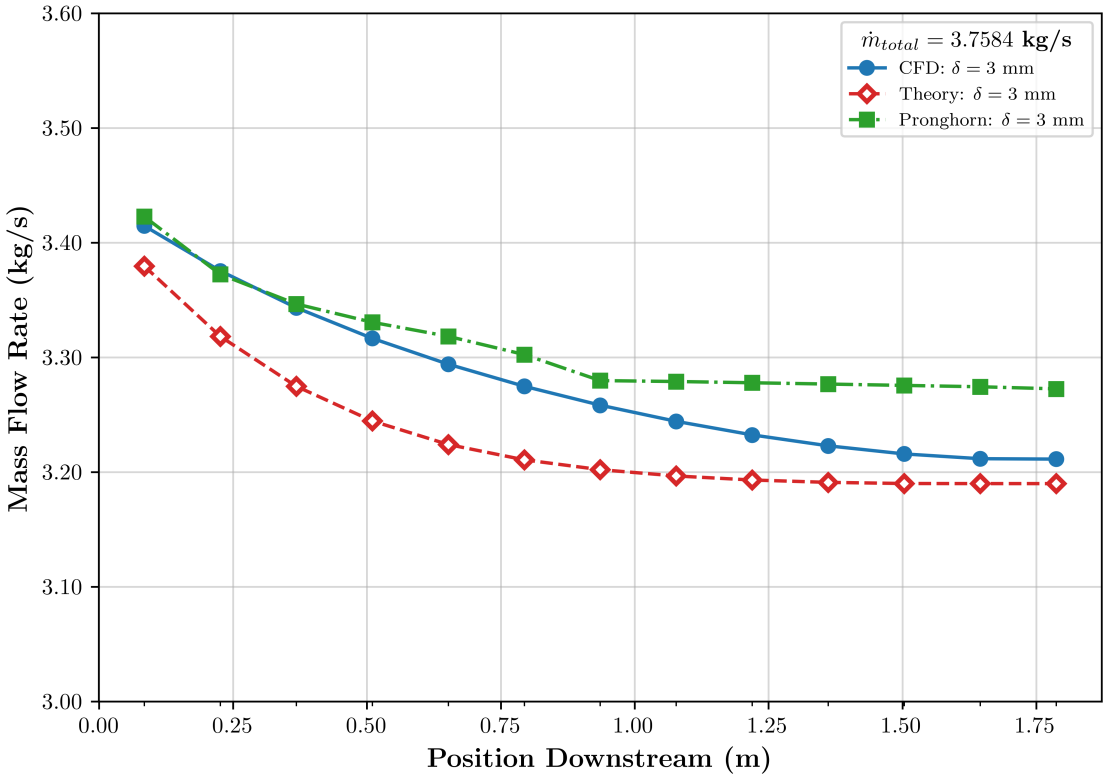

Figure 6.8: Comparison of Pronghorn, CFD, and theoretical model solutions of primary mass flow rate at each 3 mm gap downstream of the PBR inlet

Evaluating the Pronghorn results show that accounting for bypass flow is feasible, however, some challenges presented required simplification of the Pronghorn model. For the computational domain, it was necessary to neglect the presence of the cavity and only model the pebble bed. As the coolant flows from the empty cavity region into the pebble bed, the change in porosity at the interface between the two regions creates large instabilities in the mass flow rate results and difficulties with convergence. Future work is necessary to fix this issue to adequately model an entire PBR domain. Another concern from Pronghorn stems from observing Fig. (6.8), where it can be seen that a smooth decreasing trend does not occur for the Pronghorn results. The difference in the results between Pronghorn and other models stems from the solid reflector that is modeled for the bypass gaps. As previously discussed, the bypass gaps are not modeled individually, which is due to difficulties achieving convergence. The solid reflector that is modeled produces results that do not properly account for removing flow from the primary region. Since the exact amount of mass flux removed into each gap is defined in Pronghorn, it is expected that the results should be identical with the CFD model, which is not the case. In summary, it is possible to account for bypass flow in Pronghorn, but to accurately model an entire PBR is not currently possible and improvements to the MOOSE-based application must be made. Simplified analyses utilizing a generated dataset are shown to be possible with reasonable results, but further development of Pronghorn is necessary and continues to be a work in progress.

7. FUTURE WORK

Need to characterize bypass flow is of utmost importance to advance the development of potential PBR designs for commercial deployment. A representative PBR model has been developed for CFD investigations, the first part of a two-step approach for PBR bypass studies. Modeled after the HTR-10, the PBR domain simulates fluid flow through the reactor core, horizontal and vertical gaps. Considering gap sizes of 1 mm, 2 mm and 3 mm of constant width, several simulations were performed investigating potential phenomena that had an impact on bypass flow. The results obtained from the CFD investigation using the commercial CFD software, STAR-CCM+, show promise with thermal-hydraulics and porous media theory. It is apparent that the gap size plays a key role on controlling the amount of bypass flow present in the PBR domain. Other studies, however, have shown that there is little to no significance when varying parameters such as the mass flow rate. We do not imply that mass flow rate always has an effect of bypass flow, but our results indicate that it sometimes does. This warrants further investigation, whether it be with varied gap sizes, a larger range of mass flow rate values, or other properties that may be of importance but are yet to be determined.

The designation above for future work also leads to a need for consideration of how various regions considered in a PBR model can have an a effect on the overall distribution of the flow in the system. The representative PBR model in this study has assumptions made for simplicity in regards to the computational domain that must be considered in future investigations. The representative PBR model was developed with assumptions neglecting the conus, lower plenum, and core components. Future investigations should be conducted with the inclusion of at least the lower plenum, where the bypass flow path exists between the hot plenum and bottom plenum, otherwise referred to as the carbon brick bypasses. In this region four ducts are present, where previous literature has reported approximately 10% of the total reactor coolant traverses through [16], raising the issue of not only how much bypass flow is present in the HTR-10, but how several regions correspond to the distribution of the flow in the reactor. This suggestion for investigation

has also been made in the HTGR performance benchmark published by the International Atomic Energy Agency (IAEA) [72], reiterating the importance of the issue.

In addition to the recommendations above, the results obtained in this study serve as a foundation for a larger dataset needed to accurately assess bypass flow phenomena and develop a correlation that considers the important properties that influence bypass flow. A universal correlation that accounts for the mass redistribution in a PBR will require further analysis of bypass flow using a CFD software such as Star-CCM+, with several studies that vary parameters of interest that may alter resulting distribution into the bypass region. These further studies should evaluate a number of parameters to the development of bypass flow including height of the bed, varying gap size, and operating conditions, among others. Performing further studies using this approach, however, does not allow for validating the accuracy of results. As previously mentioned, lack of high quality validation data raises concern regarding the feasibility of the dataset constructed. In result, simulations were conducted and evaluated based on physics that have a large knowledge base so the feasibility of CFD data could be addressed. This leads to the need in future work to conduct studies with data of higher quality, which can be performed using a CFD model such as Direct Numerical Simulations (DNS). DNS is a complete model that can provide improved physics since its constituent equations are free from flow-dependent specifications [73]. DNS requires computationally extensive costs, but would satisfy an effort to have more reliable training data with improved physics.

The final recommendation for future work addresses Pronghorn and its current capabilities. The current state of this research establishes Pronghorn's ability to account for bypass flow in its current incarnation, however, with the challenges presented to perform the investigation, improvements to capabilities of the MOOSE-based application are necessary. In result, the Pronghorn model had multiple considerations to achieve feasible results and satisfy convergence criteria. First, consideration of only the pebble bed and neglecting the presence of the cavity in the PBR core was performed due to issues that arise when evaluating mass flow rate in the core at the interface between the cavity and pebble bed. The cavity is demonstrated to experience an

insignificant amount of pressure loss, but upon entering the pebble bed, a large pressure gradient is introduced. This pressure jump due to porosity results in instabilities when evaluating mass flow rate in the core, especially nearing the interface between the two regions. The porosity pressure jump increases mass flow rate significantly near the end of the cavity that is not representative of the physics that occur in the PBR. Second, the bypass gaps that are adjacent to the cavity and pebble bed were modeled as a single reflector block with solid material to conduct the study. Modeling each gap individually led to issues with achieving convergence, thus resulting in great difficulty or even the inability to produce results pertaining to bypass flow. Both of these assumptions were made due to challenges with convergence regarding the governing porous media equations, which have been documented in the Pronghorn manual with an alternate approach. The porous media governing equations have been reported to become stiff and difficult to converge in near-wall regions where $\epsilon = 0$ or 1, thus resulting in the recommendation that a simpler porosity profile or a non-unity wall porosity can help convergence [74]. With the issues at hand, it is recommended that improved capabilities of the solvers in Pronghorn are considered and the use of FVM is implemented. It is not impossible to create a T/H code that uses FEM for CFD, as several commercial software packages using FEM are currently available, such as COMSOL [75] and FLOTRAN [76]. Even with success using FEM, the reason for FVM implementation is due to several benefits that have been shown in past studies in several fields when comparing commercial codes with FEM and FVM. In summary, using FVM can result in lower relative errors, computational time, memory requirements, and a better approximation to theory in some cases [77, 78, 79, 80]. The benefits of using FVM have already been recognized by Pronghorn developers, as FVM implementation is currently underway.

With several tasks recommended for future work, this study serves as a basis for continuing investigations regarding bypass flow. Several considerations must be made in each approach to these investigations, all possessing their own challenges along the way. Due to the complexity of this phenomenon, several studies will be required to gain a greater understanding of bypass flow in the PBR.

8. CONCLUSION

As mentioned in Section (1), the present research sets out to establish methodology for improving trusted T/H modeling to characterize bypass flow phenomena. With development of potential PBR concepts rapidly underway to satisfy INL's NRIC advanced reactor pipeline vision, computationally efficient tools are necessary to perform a number of investigations in the time allotment designated. T/H codes have proven to be an adequate solution for PBR development with capabilities of running simulations in a fraction of the time compared to CFD, however, these low-fidelity codes can lack the ability to account for local phenomena and important characteristics of bypass flow. For this reason, CFD remains as a suitable approach to capture an assortment of fluid flow and heat transfer phenomena to evaluate mass redistribution in the PBR, yet the extensive computational resources required still remain a concern. With this conclusion, the primary intended contribution of this research sets out to establish methodology for improving capabilities applicable to lower-fidelity T/H tools such as Pronghorn to conduct future investigations with significantly less computational requirements and reasonable accuracy.

The present research conducted several investigations regarding bypass flow with the intent of providing the following contributions:

I. Produce a representative PBR model to perform numerous CFD studies, with the aim of generating a training dataset for use in the MOOSE-based T/H simulation tool, Pronghorn

II. Develop a model with an analogous PBR domain that obtains bypass flow distributions to support the feasibility of training data generated by CFD simulations

III. Utilize the dataset formulated by establishing an ad-hoc procedure that allows Pronghorn to perform bypass flow analyses

The contributions described above are fulfilled with several tasks to ensure an accurate PBR model is constructed and the results obtained are adequate for use in Pronghorn. The several

studies performed in this current research analyze various parameters of interest to determine the gravity it may play considering overall bypass flow presence in the system. Prior to generating a training dataset and approach for implementation into Pronghorn, a number of challenges are faced to satisfy each contribution. For instance, the analyses performed in STAR-CCM+ allow for a dataset to be constructed for use in other tools, but a lack of high quality validation data leads to the reasonable query concerning the CFD studies performed. This concern is addressed with development of an theoretical model that computes the distribution of bypass flow in each gap of a PBR domain analogous to CFD models. With a training dataset considered appropriate, other tasks must be performed to develop an approach for use in Pronghorn. In summary, to establish beneficial progress towards the aforementioned contributions, the basis of this study consisted of several tasks in respect to bypass flow analysis:

i. Create a representative PBR model with appropriate assumptions to conduct several CFD studies with reasonable computational cost

ii. Analyze the impact of multiple parameters in respect to bypass flow distribution with CFD data

iii. Develop an theoretical model that computes bypass flow rates in each gap of the PBR domain analogous to CFD studies

iv. Evaluate CFD investigations in comparison to obtained data from theoretical model

v. Construct a training dataset with applicable data obtained from the STAR-CCM+ CFD simulations for use in Pronghorn

vi. Establish an implemented approach to use CFD data in Pronghorn to compute bypass flow distribution

vii. Form a Pronghorn demonstration case displaying bypass flow distribution in a PBR

viii. Compare the Pronghorn demonstration case to the STAR-CCM+ reference to demonstrate the feasibility of computing bypass flow distribution

From the tasks performed in this research, various bypass flow phenomena is evaluated and a training dataset is formulated for use in Pronghorn. By devising an approach to utilize the dataset in Pronghorn and consequently performing multiple bypass flow investigations, the scope of this study is satisfied. In result, multiple parameters of interest that relate to bypass flow are evaluated and the significance of each parameters contribution to bypass flow is assessed. Bypass flow studies in Pronghorn demonstrate the ability to account for the distribution of this phenomenon, and with the current progress made, a recommended approach to these efforts are discussed below.

To conclude the investigation regarding bypass flow, models perform studies with varying mass flow rate from 60% to 140% under normal operation as well as consider gap sizes of $\delta = 1, 2, 3$ mm. In general, each model was successful displaying an ability to account for bypass flow phenomena with a representative PBR model based on the HTR-10. Each model used to conduct bypass flow investigations use methodology that could be utilized to the program of use, however, all three approaches varied in how the bypass flow phenomenon is accounted for. The purpose of this investigation is not to demonstrate that multiple tools can use the same method though, but rather the feasibility of computing bypass flow, and significant characteristics. From the studies mentioned, it can be observed that the major contributor to bypass flow is the size of bypass gaps, as 1 mm gaps only result in about 1% of the flow removed from the primary region, but increasing gap size to 3 mm shows 14% bypass flow. This reiterates the concern of understanding how deformation of graphite blocks occurs over a period of operation, as bypass flow will increase when the gaps between the graphite blocks increase. The small variation in gap sizes display the significance in bypass flow that can be increased, but the total mass flow rate varied from 60% to 140% results in just the opposite. For the range that was considered, there was only a very small percentage of change in the bypass flow, giving reason that any change in total mass flow rate during operation is not as concerning as the gap size. This observation could be applicable to PBRs in general, or just to the representative PBR modeled, further investigation will need to be considered.

To satisfy the tasks at hand for this research, steps form the basis of the study. The first step

involves using CFD to form a training dataset for implementation and further use in Pronghorn. The second step develops an theoretical model to compute the bypass flow rate in each gap for comparison with the training data obtaining in STAR-CCM+. The third step is formulating an approach for use of the training data in Pronghorn and successfully executing bypass studies with said data. The first step to this study as discussed briefly, was developing a training dataset, which was made possible with Star-CCM+ and the porous media modeling that considered a thermal non-equilibrium for results representative of the PBR. To summarize the evaluation, it was observed that the mass flow rate decrease or increase by 40% had little to no effect on the bypass distribution in the reactor. On the contrary, gap sizes play a significant role in the amount of bypass flow present in a PBR. This conclusion is consistent with concerns that are currently present for PBR designs, and reiterates a need for detailed investigations of a PBR model with high-fidelity computational tools or experimental data representative of a PBR design for validation purposes. Since it is nearly impossible to measure the bypass flow rate in a PBR, the impact of bypass flow when gap size grows only 1 mm is concerning due to the possibility of deformation that can be attributed to thermal or irradiation effects. Considering that it is not possible to measure bypass flow presently for a PBR, if a 6% increase in bypass flow is feasible, then depending on the period a reactor is operating, the deformation of the graphite blocks could lead to playing a signficant role on the bypass flow. The graphite blocks are not expected to alter the bypass flow paths by a full mm in PBR literature, but to the author's knowledge, the expected changes to the graphite blocks over a period of operation has not been discussed in detail.

The theoretical model developed using MATLAB and the MathWorks Optimization Toolbox™ computes the bypass flow for each gap in the PBR domain analogous to the representative PBR used in STAR-CCM+. By comparison, the trends that show loss of flow from the primary region in both the cavity and the pebble bed agree with training data obtained using CFD. With this agreement from computing bypass flow using two different methods, the training dataset is determined to be feasible and can be used in Pronghorn. By satisfying step 2, it should be noted that the test data for bypass flow is assumed to be feasible by comparison with the

theoretical model in Table (6.4) and Fig. (6.6). The data appears to agree well with each other, however, it is not assumed to be completely representative of the physics in the HTR-10 due to the simplifications made for the computational domain and a lack of validation data. With the trends observed from the data presented in this research, future work should include these investigations with a more detailed analysis using computational tools capable of capturing the physics with greater accuracy.

Regarding the third and final step, consideration of several approaches in Pronghorn for removal of primary flow from the pebble bed were attempted, presenting a number of challenges. Ultimately an approach was conducted leading to successful removal of bypass flow by a 'PiecewiseConstantFunction' and Dirichlet BC to an adjacent solid in Pronghorn. The ad-hoc approach for using CFD data in Pronghorn printed mass flux values from the dataset obtained in Star-CCM+, depending on the preferred gap size or mass flow rate. These values consisted of 2 arrays, one with the defined heights in the core where each bypass gap is located, and a second array that defines the amount of bypass flow that enters each gap downstream of the PBR inlet. The bypass flow is not computed as a cumulative value in this case, as the value entering each specific gap is used for defining in Pronghorn and imperative in accurately accounting for the amount of flow that departs the primary flow region. In a simplified summary of the ad-hoc approach, all values recorded from CFD simulations were placed into a directory referred to as a training dataset for bypass flow investigations. With the use of Python, the dataset is defined as a library allowing for parameters of interest to be obtained fairly quickly if the CFD simulation is already completed and all necessary data is tabulated. For all 19 gaps, the appropriate velocity, mass flow rate, and mass flux are stored in the training dataset to supply in Pronghorn when necessary.

With the ad-hoc approach determined to allow Pronghorn to account for the bypass flow distribution in the representative PBR, a demonstration case was formed in Pronghorn representative of the HTR-10 pebble bed. The lack of cavity in the model is attributed to difficulties with the porosity jump between a non-porous and porous interface, to be discussed in

future work suggestions. The difficulties from the resulting porosity jump led to oscillations of the fluid near the interface and difficulties with convergence. In result, the pebble bed is only considered with an adjacent reflector block modeled as a solid to represent the bypass flow region. Consequently, Pronghorn utilized the training dataset mass flow rates for each bypass gap only in the pebble bed, succesfully removing helium from the primary flow region as shown in Fig. (6.8). The results tabulated in Table (6.5) displayed roughly a 2% difference between the CFD training data, the optimization model, and the generated results. In result, Pronghorn demonstrates the ability to account for bypass flow in a PBR, however, when defining the exact amount removed from the system, the results were expected to be closer or nearly identical with the CFD results. Nevertheless, an approach using CFD to acquire a dataset for an ad-hoc approach using Pronghorn was performed and evaluated by comparison of primary flow in the pebble bed. This task was one of the objectives of this research, and although the application of bypass flow removal in Pronghorn was relatively simple, it demonstrates the feasibility that Pronghorn can remove mass flow from the system, however, some considerations need to be considered to refine the T/H simulation tool.

REFERENCES

[1] J. E. Kelly, "Generation iv international forum: A decade of progress through international cooperation," *Progress in Nuclear Energy*, vol. 77, pp. 240–246, 2014.

[2] T. Abram and S. Ion, "Generation-iv nuclear power: A review of the state of the science," *Energy Policy*, vol. 36, no. 12, pp. 4323–4330, 2008.

[3] T. K. Kim, "Gen-iv reactors," in *Nuclear Energy*, pp. 175–201, Springer, 2013.

[4] I. Pioro, *Handbook of Generation IV Nuclear Reactors*. Woodhead Publishing, 2016.

[5] J. C. Wagner, "National reactor innovation center overview," report, Idaho National Lab.(INL), Idaho Falls, ID (United States), 2019.

[6] U. D. of Defense, *Task Force on Energy Systems for Forward/Remote Operating Bases: Final Report*. Office of the Under Secretary of Defense for Acquisition, Technology, and Logistics, 2016.

[7] M. Nichol, "Roadmap for the deployment of micro-reactors for us department of defense domestic installations," report, Nuclear Energy Institute Washington DC United States, 2018.

[8] J. A. Vitali, J. G. Lamothe, C. J. J. Toomey, V. O. Peoples, and K. A. McCabe, "Mobile nuclear power plants for ground operations," report, HQDA G-4 Future Operations and Strategy WASHINGTON United States, 2018.

[9] B. G. Williams, R. R. Schultz, D. M. McEligot, and G. McCreery, "Studies of deteriorated heat transfer in prismatic cores stemming from irradiation-induced geometry distortion," report, Idaho National Laboratory (INL), 2015.

[10] F. Roelofs, *Thermal hydraulics aspects of liquid metal cooled nuclear reactors*. Woodhead Publishing, 2018.

[11] C. Permann, D. Gaston, D. Andrs, R. Carlsen, F. Kong, A. Lindsay, J. Miller, J. Peterson, A. Slaughter, R. Stogner, and R. Martineau, "Moose: Enabling massively parallel multiphysics simulation," *Preprint submitted to SoftwareX*, 2020.

[12] A. Novak, S. Schunert, R. Carlsen, P. Balestra, R. Slaybaugh, and R. Martineau, "Multiscale thermal-hydraulic modeling of the pebble bed fluoride-salt-cooled high-temperature reactor," *Annals of Nuclear Energy*, vol. 154, p. 107968, 2021.

[13] E. López-Honorato, J. Tan, P. Meadows, G. Marsh, and P. Xiao, "Triso coated fuel particles with enhanced sic properties," *Journal of nuclear materials*, vol. 392, no. 2, pp. 219–224, 2009.

[14] Q. Zhenya, "The general design of the 10mw htr," in *The 3rd JAERI Symposium on HTGR*, 1996.

[15] J. J. Powers and B. D. Wirth, "A review of triso fuel performance models," *Journal of Nuclear Materials*, vol. 405, no. 1, pp. 74–82, 2010.

[16] S. Sun, Y. Zhang, and Y. Zheng, "Research on influence of different simulation methods of bypass flow in thermal hydraulic analysis on temperature distribution in htr-10," *Science and Technology of Nuclear Installations*, vol. 2020, p. 4754589, 2020.

[17] H. Peng and J. Sun, "Numerical investigations of the helium flow in mini-scale gaps," in *International Confernece Pacific Basin Nuclear Conference*, pp. 201–217, Springer, 2016.

[18] "Evaluation of high temperature gas cooled reactor performance: Benchmark analysis related to initial testing of the httr and htr-10," Tech. Rep. IAEA-TECDOC-1382, International Atomic Energy Agency (IAEA), Vienna, Austria, 2003.

[19] W. Wulff, B. Boyack, and R. Duffey, "Quantifying reactor safety margins: Application of csau methodology to lbloca," report, Nuclear Regulatory Commission (NRC), 1989.

[20] G. E. Wilson and B. E. Boyack, "The role of the pirt process in experiments, code development and code applications associated with reactor safety analysis," *Nuclear Engineering and Design*, vol. 186, no. 1-2, pp. 23–37, 1998.

[21] S. J. Ball, M. Corradini, S. E. Fisher, R. Gauntt, G. Geffraye, J. C. Gehin, Y. Hassan, D. L. Moses, J.-P. Renier, and R. Schultz, "Next generation nuclear plant phenomena identification and ranking tables (pirts) volume 2: Accident and thermal fluids analysis pirts," Report NUREG/CR-6944, Vol. 2, Oak Ridge National Laboratory (United States), 2008.

[22] R. Morris, D. Petti, D. Powers, B. Boyack, and M. Rubin, "Triso-coated particle fuel phenomenon identification and ranking tables (pirts) for fission product transport due to manufacturing, operations, and accidents," Report NUREG/CR-6844, Vol. 1, U.S. Nuclear Regulatory Commission, 2004.

[23] A. J. Huning, S. Chandrasekaran, and S. Garimella, "A review of recent advances in htgr cfd and thermal fluid analysis," *Nuclear Engineering and Design*, vol. 373, p. 111013, 2021.

[24] Z. Wu, D. Lin, and D. Zhong, "The design features of the htr-10," *Nuclear Engineering and Design*, vol. 218, no. 1-3, pp. 25–32, 2002.

[25] J. Janse van Rensburg, "Advances in the cfd modelling of the pbmr to improve the on of bypass flows," in *High Temperature Reactor Technology*, vol. 48548, pp. 403–410, 2008.

[26] H. Sato, R. Johnson, and R. Schultz, "Computational fluid dynamic analysis of core bypass flow phenomena in a prismatic VHTR," *Annals of Nuclear Energy*, vol. 37, pp. 1172–1185, sep 2010.

[27] R. W. Johnson and H. Sato, "Bypass flow computations using a one-twelfth symmetric sector for normal operation in a 350mwth prismatic VHTR," *Nuclear Engineering and Design*, vol. 251, pp. 84–91, oct 2012.

[28] J. J. Janse van Rensburg and M. Kleingeld, "A cfd method to evaluate the integrated influence of leakage and bypass flows on the pbmr reactor unit," *Nuclear Engineering and Design*, vol. 240, no. 11, pp. 3841–3850, 2010.

[29] J. J. van Rensburg and M. Kleingeld, "Investigating leakage and bypass flows in an HTR using a CFD methodology," *Nuclear Engineering and Design*, vol. 241, pp. 4960–4971, dec 2011.

[30] J. J. Janse van Rensburg and M. Kleingeld, "Cfd applications in the pebble bed modular reactor project: A decade of progress," *Nuclear Engineering and Design*, vol. 241, no. 9, pp. 3683–3696, 2011.

[31] J. Sun, Y. Zheng, F. Li, Z. Sui, and Y. Ma, "Prediction of bypass flows in the htr-pm by the flow network method," in *International Conference on Nuclear Engineering*, vol. 43900, American Society of Mechanical Engineers, 2011.

[32] J. Sun, Y. Zheng, and F. Li, "Various bypass flow paths and bypass flow ratios in htr-pm," *Energy Procedia*, vol. 39, pp. 258–266, 2013.

[33] J. Sun, Y. Zheng, and F. Li, "Bypass flows in control rod channels of the htr-pm," in *International Conference on Nuclear Engineering*, vol. 55812, p. V004T09A002, American Society of Mechanical Engineers, 2013.

[34] J. Sun, Z. Chen, Y. Zheng, L. Shi, and F. Li, "Predictions of the bypass flows in the htr-pm reactor core," in *International Conference on Nuclear Engineering*, American Society of Mechanical Engineers, 2014.

[35] Z. Liu, Z. Li, and J. Sun, "Bypass flow in small absorber sphere channels of the high-temperature gas-cooled reactor pebble-bed module," *The Journal of Computational Multiphase Flows*, vol. 10, no. 3, pp. 128–139, 2017.

[36] X. Sun, Z. Chen, J. Sun, Y. Liu, Y. Zheng, F. Li, and L. Shi, "CFD investigation of bypass flow in HTR-PM," *Nuclear Engineering and Design*, vol. 329, pp. 147–155, apr 2018.

[37] H. K. Versteeg and W. Malalasekera, *An introduction to computational fluid dynamics: the finite volume method*. Pearson education, 2007.

[38] W. Jones and B. E. Launder, "The prediction of laminarization with a two-equation model of turbulence," *International journal of heat and mass transfer*, vol. 15, no. 2, pp. 301–314, 1972.

[39] T.-H. Shih, W. W. Liou, A. Shabbir, Z. Yang, and J. Zhu, "A new $k - \epsilon$ eddy viscosity model for high reynolds number turbulent flows," *Computers & Fluids*, vol. 24, no. 3, pp. 227–238, 1995.

[40] M. van Staden, C. Van Rensburg, and L. Le Grange, "Thermo-hydraulic modeling of heat removal for the pbmr helium gas cooled reactor using cfd," in *Proceedings of International Congress on Advances in Nuclear Power Plants (ICAPP'03)*, 2003.

[41] J. Janse van Rensburg, C. Viljoen, and M. Van Staden, "Cfd modeling of high temperature gas cooled reactors," in *Proceedings of the 2006 international congress on advances in nuclear power plants-ICAPP'06*, 2006.

[42] J. J. Janse van Rensburg and M. Kleingeld, "An integral cfd approach for the thermal simulation of the pbmr reactor unit," *Nuclear Engineering and Design*, vol. 241, no. 8, pp. 3130–3141, 2011.

[43] S. CD-Adapco, "Star-ccm+ user guide version 15.06," *CD-Adapco: New York, NY, USA*, 2021.

[44] S. V. Patankar, *Numerical Heat Transfer and Fluid Flow*. Hemisphere Publishing Corporation, 1980.

[45] C. Rhie and W. L. Chow, "Numerical study of the turbulent flow past an airfoil with trailing edge separation," *AIAA journal*, vol. 21, no. 11, pp. 1525–1532, 1983.

[46] F. Moukalled, L. Mangani, and M. Darwish, *The finite volume method in computational fluid dynamics*, vol. 6. Springer, 2016.

[47] R. W. Johnson, "Modeling strategies for unsteady turbulent flows in the lower plenum of the vhtr," *Nuclear Engineering and Design*, vol. 238, no. 3, pp. 482–491, 2008.

[48] H. Petersen, "The properties of helium: density, specific heats, viscosity, and thermal conductivity at pressures from 1 to 100 bar and from room temperature to about 1800 k," *RISO-DTU*, vol. 224, 1970.

[49] K. Ausschuss, "Kta 3102.1 reactor core design for high-temperature gas-cooled reactor part 1: Calculation of the material properties of helium," report, Nuclear Safety Standards Commission (KTA), 1978.

[50] J. Bear, *Dynamics of fluids in porous media*. Courier Corporation, 2013.

[51] A. Fluent, "12.0 theory guide," *Ansys Inc.*, vol. 5, no. 5, p. 15, 2009.

[52] R. O. Scarlat, *Design of Complex Systems to Achieve Passive Safety: Natural Circulation Cooling of Liquid Salt Pebble Bed Reactors*. Thesis, UC Berkeley, 2012.

[53] K. Ausschuss, "Kta 3102.3 reactor core design for high-temperature gas-cooled reactor part 3: Loss of friction in pebble bed cores," report, Nuclear Safety Standards Commission (KTA), 1981.

[54] G. Breitbach and H. Barthels, "The radiant heat transfer in the high temperature reactor core after failure of the afterheat removal systems," *Nuclear Technology*, vol. 49, no. 3, pp. 392–399, 1980.

[55] C. Ren, X. Yang, H. Jia, Y. Jiang, and W. Xiong, "Theoretical analysis of effective thermal conductivity for the chinese htr-pm heat transfer test facility," *Applied Sciences*, vol. 7, no. 1, p. 76, 2017.

[56] I. A. E. Agency, "Evaluation of high temperature gas cooled reactor performance: benchmark analysis related to the pbmr-400, pbmm, gt-mhr, htr-10 and the astra critical facility," 2013.

[57] R. Masterson, *Nuclear Reactor Thermal Hydraulics: An Introduction to Nuclear Heat Transfer and Fluid Flow*. CRC Press, 2019.

[58] S. Boyd, S. P. Boyd, and L. Vandenberghe, *Convex optimization*. Cambridge university press, 2004.

[59] A. Messac, *Optimization in practice with MATLAB®: for engineering students and professionals*. Cambridge University Press, 2015.

[60] Y. Li, "Centering, trust region, reflective techniques for nonlinear minimization subject to bounds," report, Cornell University, 1993.

[61] The Mathworks Inc., 1 Apple Hill Dr., Natick, MA, 01760-2098, *MATLAB Optimization Toolbox*, r2021a ed., 2021.

[62] T. L. Bergman, F. P. Incropera, D. P. DeWitt, and A. S. Lavine, *Fundamentals of heat and mass transfer*. John Wiley & Sons, 2011.

[63] A. Novak, R. Slaybaugh, and R. Martineau, "Multiscale core thermal-hydraulics analysis of the pebble bed fluoride-salt-cooled high-temnperature reactor (pb-fhr)," *Proceeding of Mathematics and Computational Methods Applied to Nuclear Science and Engineering, M&C*, 2019.

[64] A. Novak, J. Peterson, L. Zou, D. Andrš, R. Slaybaugh, and R. Martineau, "Validation of pronghorn friction-dominated porous media thermal-hydraulics model with the sana experiments," *Nuclear Engineering and Design*, vol. 350, pp. 182–194, 2019.

[65] A. J. Novak, L. Zou, J. W. Peterson, R. Martineau, and R. Slaybaugh, "Pronghorn: Porous media thermal-hydraulics for reactor applications," *Transactions of the American Nuclear Society*, vol. 119, pp. 175–178, 2018.

[66] A. Novak, *Multiscale Thermal-Hydraulic Methods for Pebble Bed Reactors*. Thesis, UC Berkeley, 2020.

[67] J. N. Reddy, *An Introduction to Nonlinear Finite Element Analysis Second Edition: with applications to heat transfer, fluid mechanics, and solid mechanics*. Oxford University Press, 2014.

[68] B. Boer, D. Lathouwers, J. Kloosterman, T. Van Der Hagen, and G. Strydom, "Validation of the dalton-thermix code system with transient analyses of the htr-10 and application to the pbmr," *Nuclear technology*, vol. 170, no. 2, pp. 306–321, 2010.

[69] A. G. Rodríguez, L. Y. R. Mazaira, C. R. G. Hernández, D. S. Dominguez, and C. A. B. de Oliveira Lira, "An integral 3d full-scale steady-state thermohydraulic calculation of the

high temperature pebble bed gas-cooled reactor htr-10," *Nuclear Engineering and Design*, vol. 373, p. 111011, 2021.

[70] B. Li, Z. Gao, and Z. Jiang, "Steady thermohydraulic analysis of 10 mw htgr," *Chinese Journal of Nuclear Science and Engineering*, vol. 13, no. 4, pp. 69–76, 1993.

[71] Z. Gao and L. Shi, "Thermal hydraulic calculation of the htr-10 for the initial and equilibrium core," *Nuclear Engineering and Design*, vol. 218, no. 1-3, pp. 51–64, 2002.

[72] "Evaluation of high temperature gas cooled reactor performance: Benchmark analysis related to the pbmr-400, pbmm, gt-mhr, htr-10 and the atra critical facility," Tech. Rep. IAEA-TECDOC-1694, International Atomic Energy Agency (IAEA), Vienna, Austria, 2013.

[73] S. B. Pope, *Turbulent Flows*. Cambridge University Pr., 2000.

[74] C. G. Du Toit, "Radial variation in porosity in annular packed beds," *Nuclear engineering and design*, vol. 238, no. 11, pp. 3073–3079, 2008.

[75] C. Multiphysics, "Introduction to comsol multiphysics®," *COMSOL Multiphysics, Burlington, MA, accessed Feb*, vol. 9, p. 2018, 1998.

[76] U. Gohner and H. Mauch, "Flotran: Numerical method and industrial applications," *International Journal of Computer Applications in Technology*, vol. 11, no. 3-5, pp. 199–202, 1998.

[77] S. Geller, M. Krafczyk, J. Tölke, S. Turek, and J. Hron, "Benchmark computations based on lattice-boltzmann, finite element and finite volume methods for laminar flows," *Computers & fluids*, vol. 35, no. 8-9, pp. 888–897, 2006.

[78] W. Ludwig and J. Dziak, "Cfd modelling of a laminar film flow," *Chemical and process engineering*, vol. 30, pp. 417–430, 2009.

[79] F. Molina-Aiz, H. Fatnassi, T. Boulard, J.-C. Roy, and D. Valera, "Comparison of finite element and finite volume methods for simulation of natural ventilation in greenhouses," *Computers and electronics in agriculture*, vol. 72, no. 2, pp. 69–86, 2010.

[80] W. Jeong and J. Seong, "Comparison of effects on technical variances of computational fluid dynamics (cfd) software based on finite element and finite volume methods," *International Journal of Mechanical Sciences*, vol. 78, pp. 19–26, 2014.

[81] A. Butland and R. Maddison, "The specific heat of graphite: an evaluation of measurements," *Journal of Nuclear Materials*, vol. 49, no. 1, pp. 45–56, 1973.

[82] B. Stöcker and H. F. Niessen, "Data sets of the sana experiment 1994-1996," report, Forschungszentrum Juelich GmbH (Germany). Inst. fuer Sicherheitsforschung, 1997.

A. PEBBLE BED REACTOR PARAMETERS

Appendix A details correlations that are applicable to characterizing PBR bypass flow and is utilized in one of the three methods employed in the present study that provide further analysis of the bypass flow phenomenon. Fluid properties for helium listed in Section (A.1.1) refer to Safety Standard KTA 3102.1 [49] from the German Nuclear Safety Standards Commission, Kerntechnischer Ausschuss (KTA). Solid properties in Section (A.1.2) refer to KTA electric graphite Sigri Al 2-500 that was previously published in a study involving polynomial fitting of nuclear graphite data over a wide range of temperatures [81], and datasets from the SANA test facility experiment [82]. The correlations published in this appendices play a key role in defining PBR models for all three computational tools used in the bypass flow investigation. For reference about porous media modeling, refer to Section (3.3.1).

A.1 Thermophysical Properties

A.1.1 Fluid Properties

$$\rho_f = 48.14 \cdot \frac{P}{T}\left(1 + 0.4446 \cdot \frac{P}{T^{1.2}}\right)^{-1} \tag{A.1}$$

$$\mu = 3.674 \cdot 10^{-7} \cdot T^{0.7} \tag{A.2}$$

$$k_f = 2.682 \cdot 10^{-3}\left(1 + 1.123 \cdot 10^{-3} \cdot P\right) \cdot T^{0.71(1-2\cdot 10^{-4}\cdot P)} \tag{A.3}$$

$$c_p = 5195 \tag{A.4}$$

$$c_v = 3117 \tag{A.5}$$

A.1.2 Solid Properties

Models for the representative PBR characterize the solid in the porous medium (i.e., fuel pebbles) as KTA electric graphite, otherwise known as Sigri Al 2-500 electric graphite. KTA electric graphite utilizes correlations for various solid material properties obtained from the references reported above. The electric graphite density, thermal conductivity, and isobaric specific heat are defined as

$$\rho_s = 1673 \;\; kg/m^3 \tag{A.6}$$

$$k_s = -22.05679 \ln(T_s) + 194.32788 \;\; W/m \cdot K \tag{A.7}$$

$$C_{p,s} = 4184\left(0.5421 + a_1 T_s - \frac{a_2}{T_s} - \frac{a_3}{T_s^2} + \frac{a_4}{T_s^3} + \frac{a_5}{T_s^4}\right) \;\; J/kg \cdot K \tag{A.8}$$

where $a_1 = -2.4267 \times 10^{-6}$, $a_2 = 90.273$, $a_3 = 43449$, $a_4 = 1.5931 \times 10^7$, and $a_5 = -1.4369 \times 10^9$.

A.2 Pebble Bed Correlations

A.2.1 KTA Pressure Loss

Loss of pressure through friction in a pebble bed is calculated using the KTA correlation provided by [[53]] for a layer of height ΔH. Pressure loss can be determined with the range,

$$\begin{cases} 0.36 < \epsilon < 0.42, \\ 1 < Re_h < 10^5, \\ D/d_p, \quad \text{Limiting Curve in [53]} \end{cases} \tag{A.9}$$

where Re_h is the hydraulic reynolds number in the pebble bed, d_p is the pebble diameter, D is the porous media hydraulic diameter. D/d_p is a limiting curve provided in the source

documentation. Satisfying the range requirement, the pressure loss is determined as,

$$\frac{\Delta P}{\Delta H} = \Psi \cdot \frac{1-\varepsilon}{\varepsilon^3} \cdot \frac{1}{d_p} \cdot \frac{1}{2\rho} \cdot \left(\frac{\dot{m}}{A}\right)^2 \tag{A.10}$$

where Ψ is the coefficient of loss of pressure through friction. The coefficient of loss of pressure through friction is calculated by,

$$\Psi = \frac{320}{\left(\frac{Re}{1-\varepsilon}\right)} + \frac{6}{\left(\frac{Re}{1-\varepsilon}\right)^{-1}} \tag{A.11}$$

where Re is the Reynolds number with consideration of the pebble diameter and superficial velocity.

A.2.2 KTA Drag Model

Pebble bed friction factors considering inertial and viscous drag scales are quantified by the KTA drag model [53], applicable within the following scope,

$$\begin{cases} 0.36 < \epsilon < 0.42, \\ 1 < Re_h < 10^5, \\ D/d_p, \quad \text{Limiting Curve in [53]} \end{cases} \tag{A.12}$$

where Re_h is the hydraulic reynolds number in the pebble bed, d_p is the pebble diameter, D is the porous media hydraulic diameter. Coefficients A and B presented in the KTA model determine the friction factor by,

$$A = 160, \tag{A.13a}$$

$$B = 3\left(\frac{Re}{1-\epsilon}\right)^{-0.1} \tag{A.13b}$$

where A and B are applicable for quantifying pressure loss due to friction in porous media.

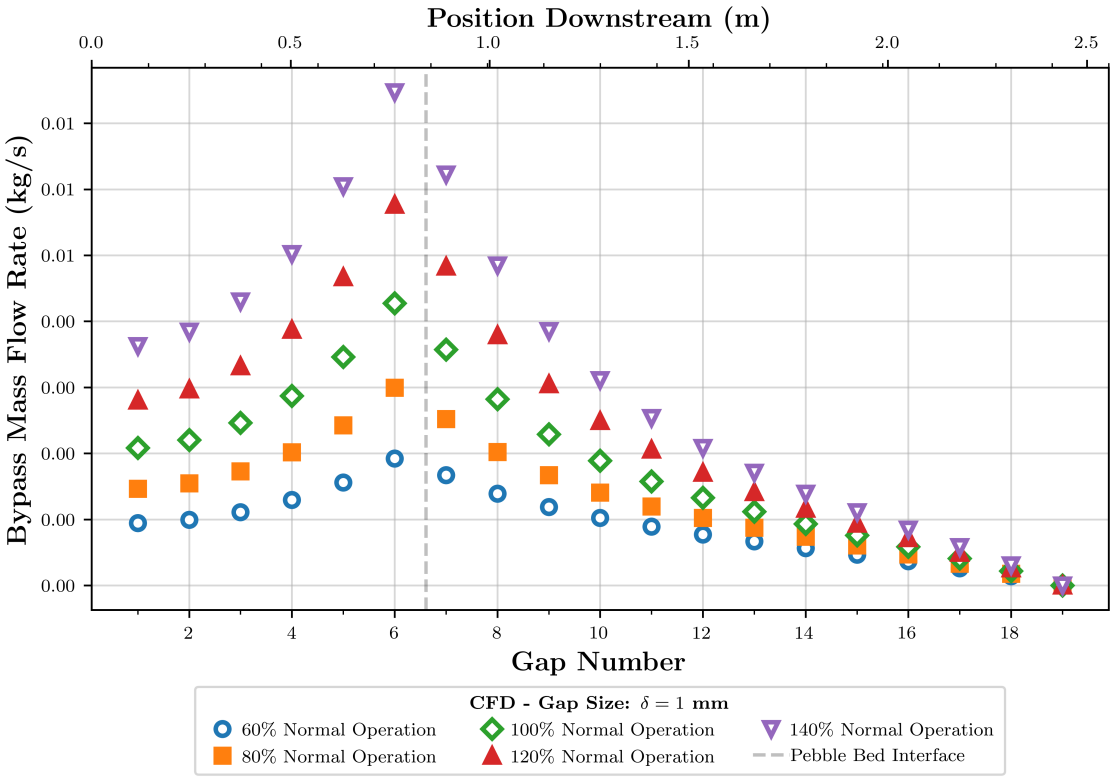

Figure B.1: Primary mass flow rate in the core for 1 mm gaps with varied mass flow rates

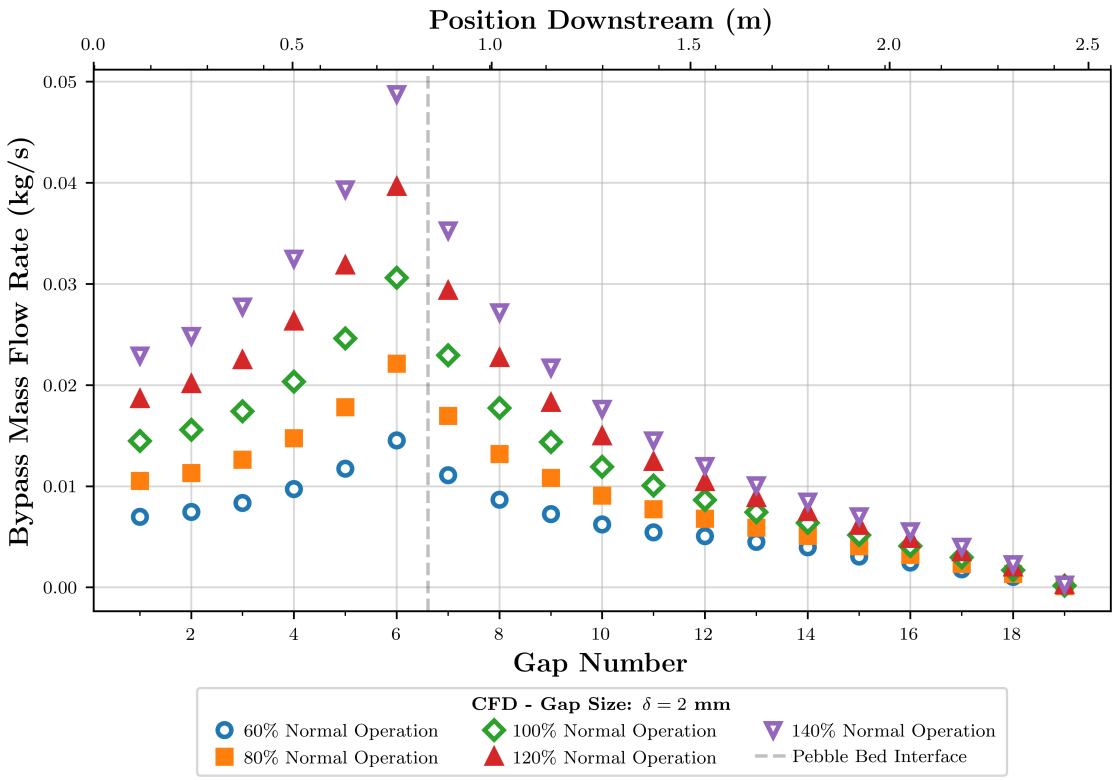

Figure B.2: Primary mass flow rate in the core for 2 mm gaps with varied mass flow rates

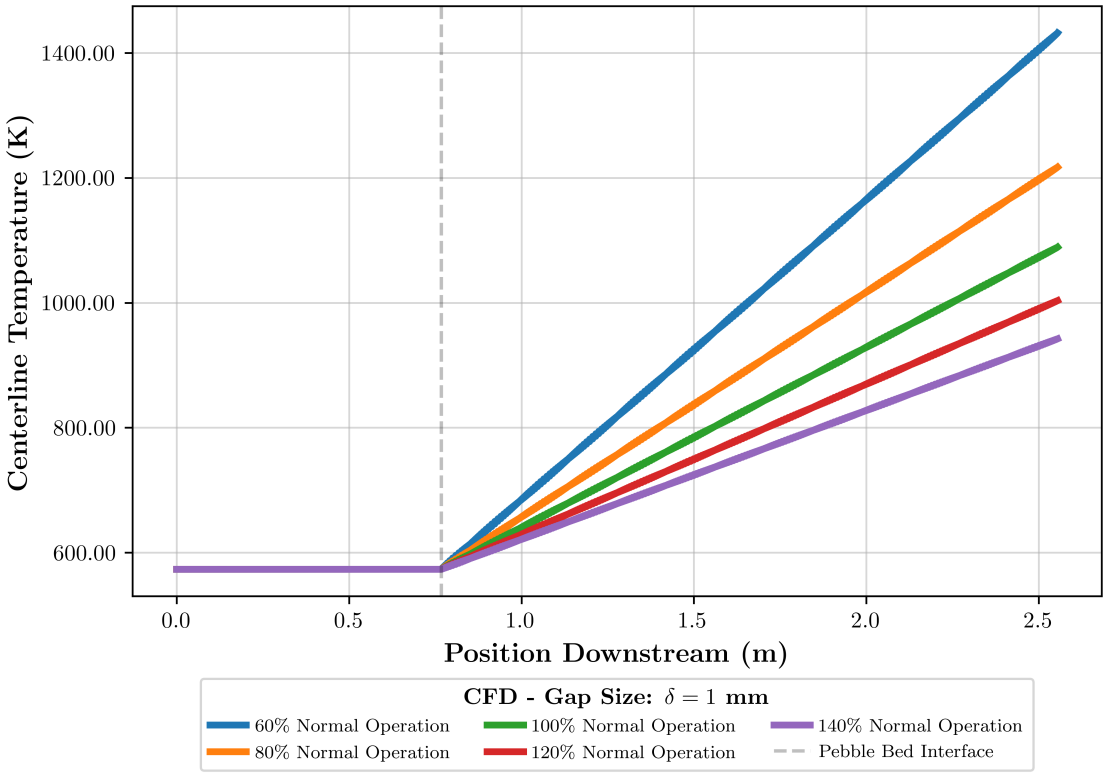

Figure B.3: Axial centerline temperature in the PBR core with 1 mm gaps for total mass flow rate cases ranging from 60% to 140% of normal operating conditions

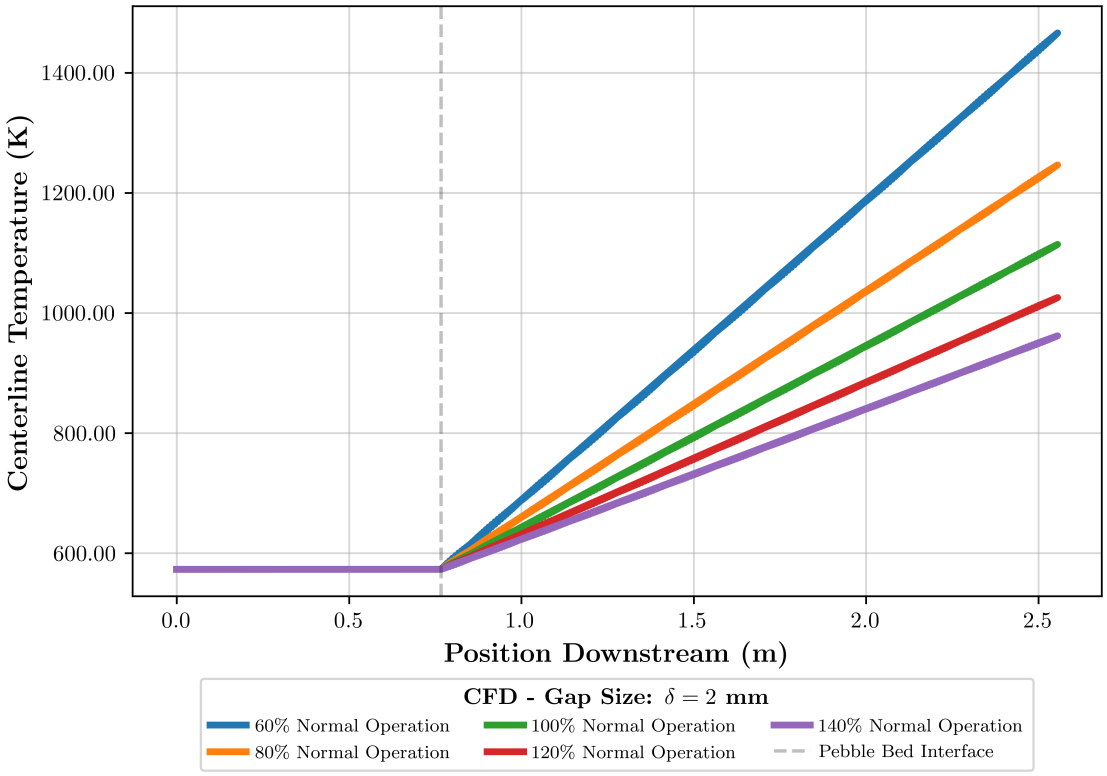

Figure B.4: Axial centerline temperature in the PBR core with 2 mm gaps for total mass flow rate cases ranging from 60% to 140% of normal operating conditions

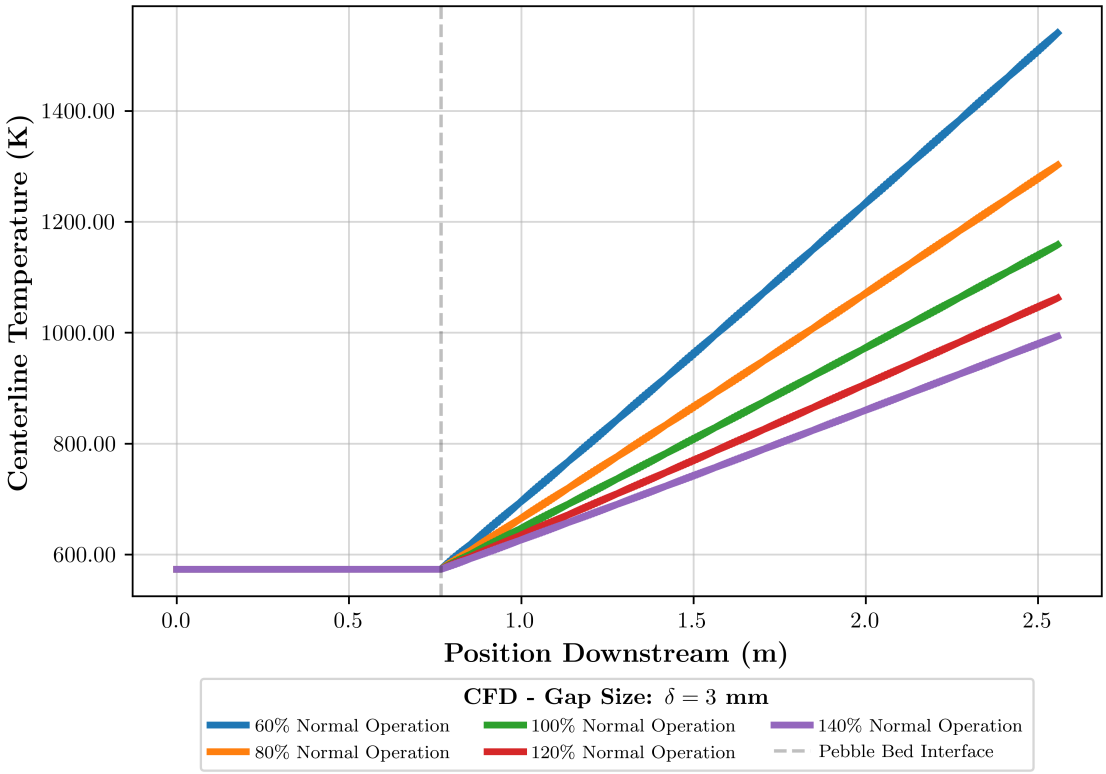

Figure B.5: Axial centerline temperature in the PBR core with 3 mm gaps for total mass flow rate cases ranging from 60% to 140% of normal operating conditions

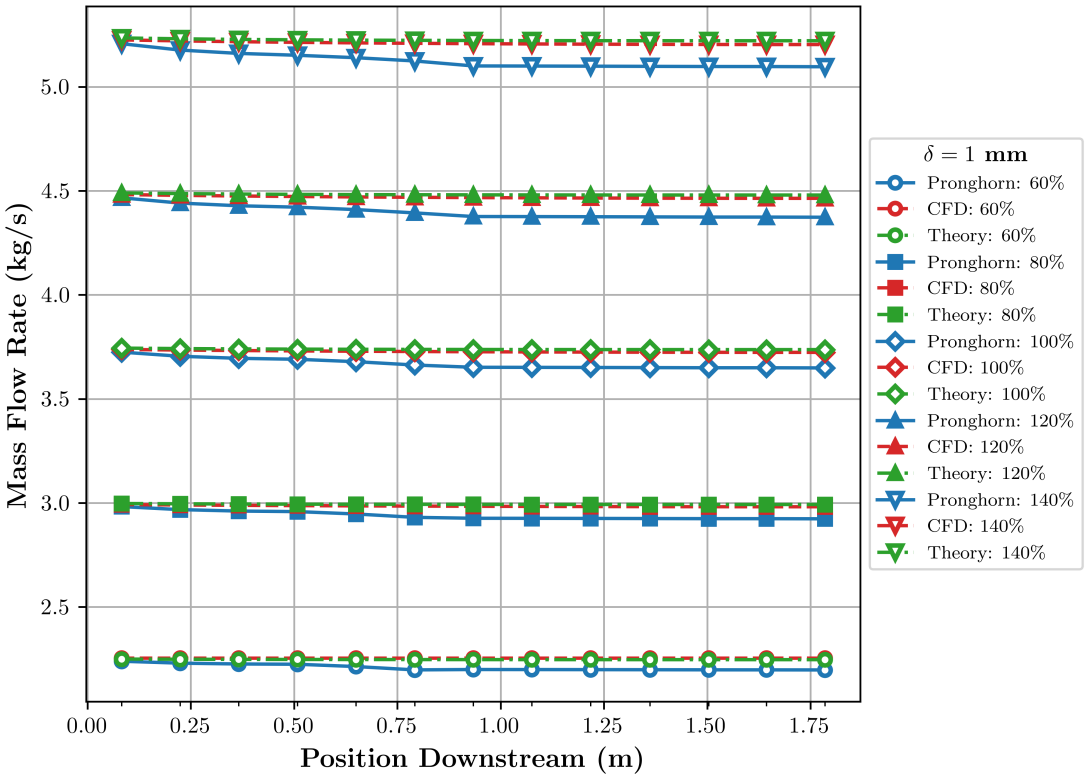

Figure B.6: Comparison of Pronghorn, validation code, and CFD results for 1 mm gaps at 100% normal operating conditions

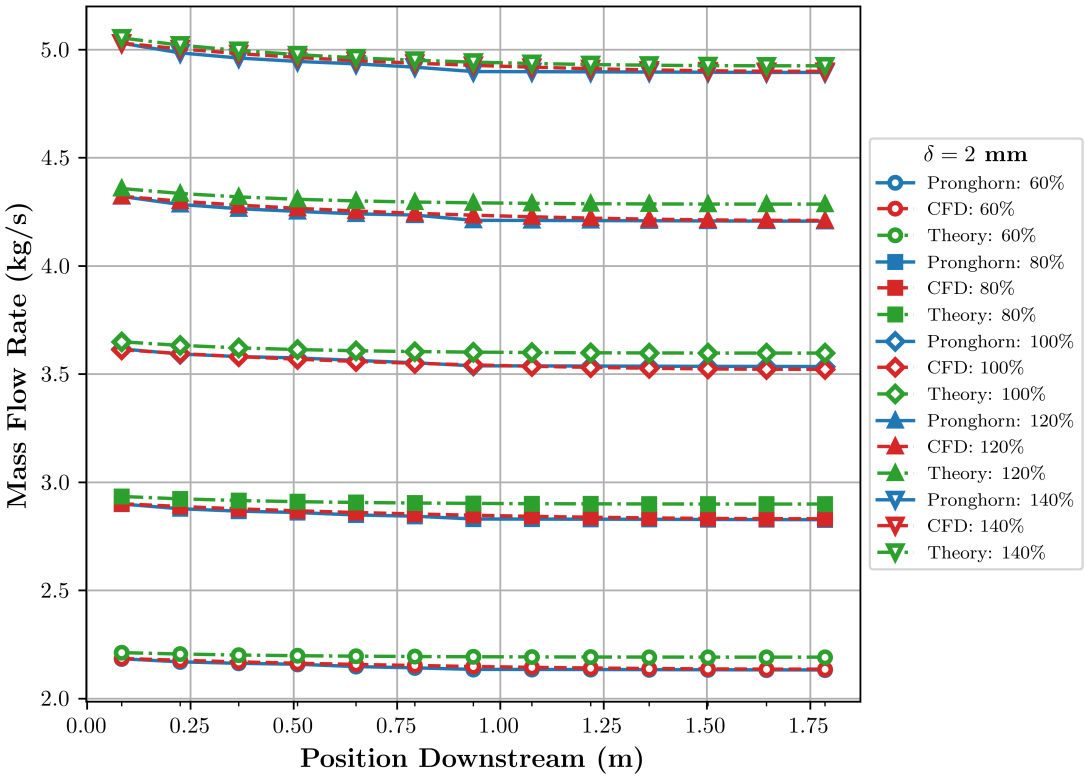

Figure B.7: Comparison of Pronghorn, validation code, and CFD results for 2 mm gaps at 100% normal operating conditions

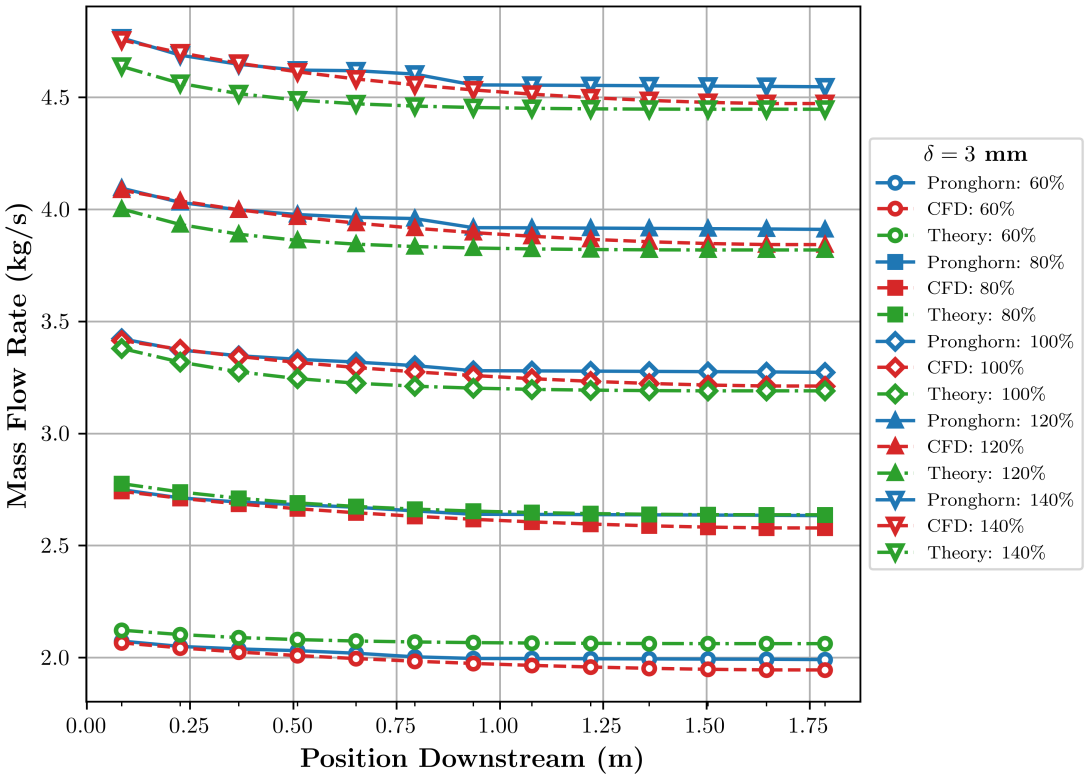

Figure B.8: Comparison of Pronghorn, validation code, and CFD results for 3 mm gaps at 100% normal operating conditions

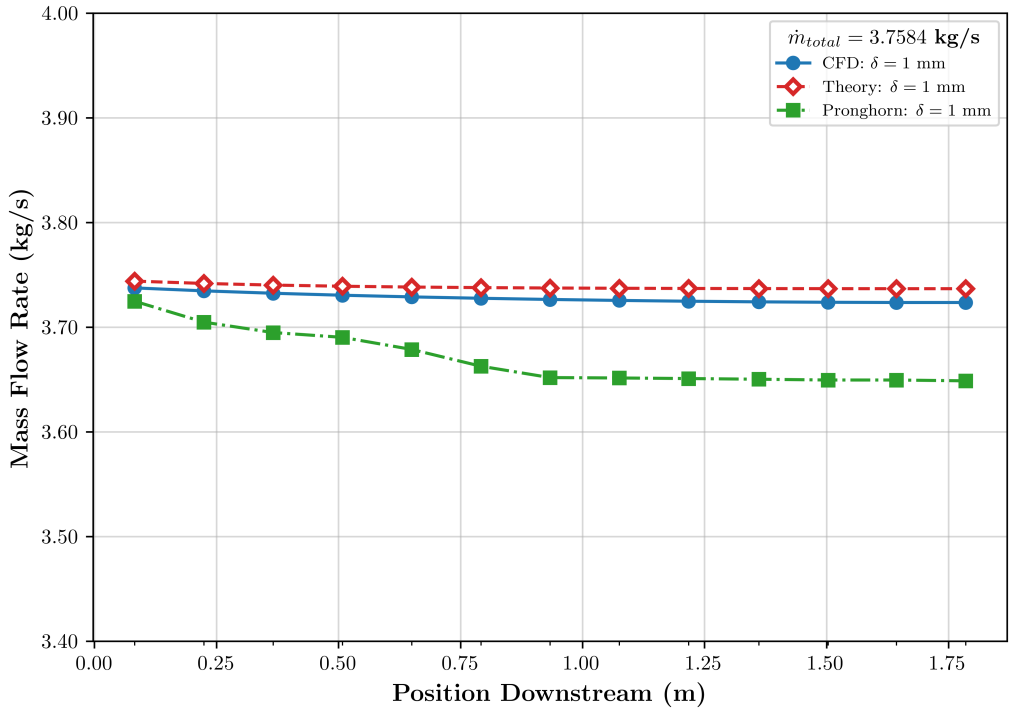

Figure B.9: Comparison Pronghorn, CFD, and the optimization model solutions of primary mass flow rate at each 1 mm gap downstream of the PBR inlet.

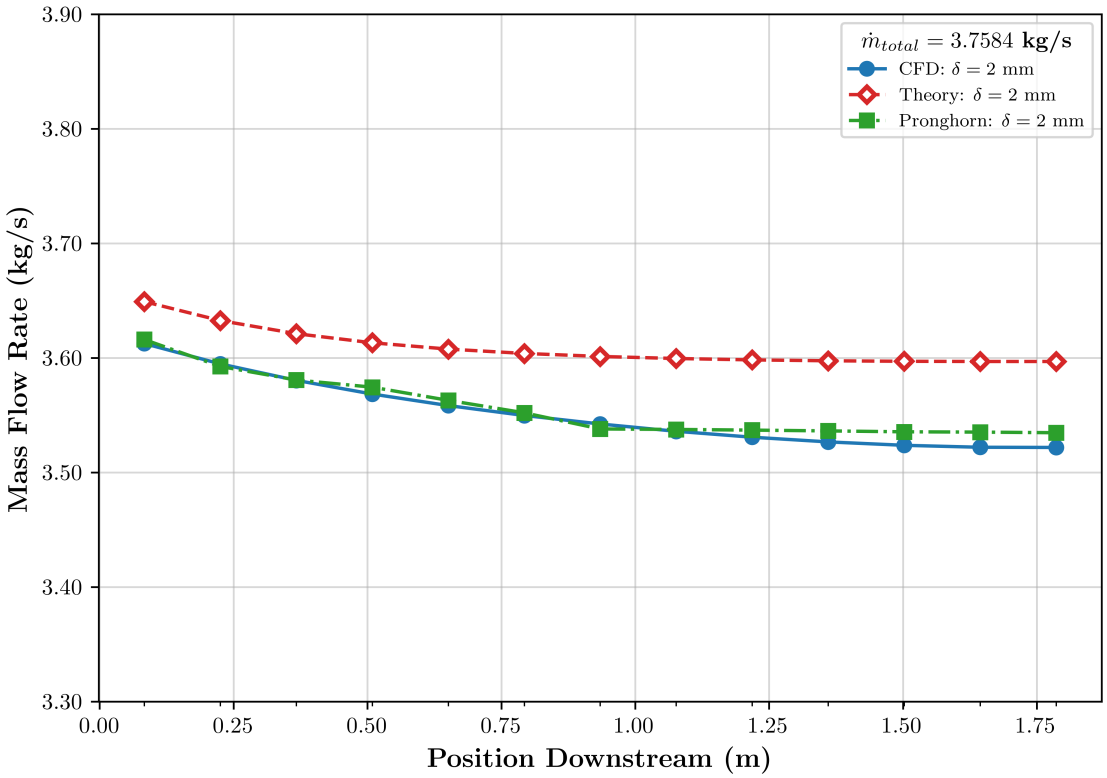

Figure B.10: Comparison Pronghorn, CFD, and the optimization model solutions of primary mass flow rate at each 2 mm gap downstream of the PBR inlet.